Temporal variations of seismicity rates and Gutenberg-Richter *b*-values for a stochastic declustered catalog: an example in central Italy

A.E. Pastoressa[1], M. Murru[1], M. Taroni[1], R. Console[1,*], C. Montuori[1], G. Falcone[1], R. Di Stefano[1]

[1] Istituto Nazionale di Geofisica e Vulcanologia (INGV), Rome, Italy

* also at: Center of Integrated Geomorphology for the Mediterranean Area, Potenza, Italy

Corresponding author:

Anna Eliana Pastoressa, address: Via di Vigna Murata 605, 00143, Rome, RM, Italy; email: annaeliana.pastoressa@ingv.it

Declaration of Competing Interests:

The authors declare no competing interests

ABSTRACT

One important aspect of the seismicity is the spatio-temporal clustering; hence, the distinction between independent and triggered events is a critical part of the analysis of seismic catalogs. Stochastic declustering of seismicity allows a probabilistic distinction between these two kinds of events. Such an approach, usually performed with the ETAS model, avoids the bias in the estimation of the frequency magnitude distribution parameters if we consider a subset of the catalog, i.e. only the independent or the triggered events. In this paper we present a framework to properly include the probabilities of any event to be independent (or triggered) both in the temporal variation of the seismic rates and in the estimation of the *b*-value of the Gutenberg-Richter law. This framework is then applied

to a high-definition seismic catalog in the central part of Italy covering the period from April 2010 to December 2015. The results of our analysis show that the seismic activity from the beginning of the catalog to March 2013 is characterized by a low degree of clustering and a relatively high *b*-value, while the following period exhibits a higher degree of clustering and a smaller *b*-value.

INTRODUCTION

The seismic hazard assessment and, in general, the capability of identifying possible correlations between the variations of the Earth crust physical properties and the space-time seismicity distribution, needs a reliable statistical analysis of the seismic catalogs. The possibility of performing reliable statistical analyses is certainly related to the use of estimation methods that must be robust and independent of the researcher's subjective choices; for this reason, we propose a series of procedures of seismic catalogs analyses characterized by a high degree of objectivity and robustness, finalized to the estimation of the seismicity rates and Gutenberg-Richter *b*-values (Gutenberg and Richter, 1944) temporal variations.

A first essential step to conduct a careful and conscious study of the seismicity, in addition to a deep knowledge of the catalog and its problems (e.g., catalog completeness), is represented by the so-called declustering process. The declustering process consists in the separation of the independent events from the earthquakes which depend on each other's (triggered events). This distinction is mainly finalized to collect different information about the earthquake potential estimation. In fact, while independent earthquakes are generally associated with secular tectonic phenomena, the triggered events are mainly attributed to stress variations caused by previous events (Aki, 1956; Knopoff, 1964). Currently, there are several approaches for declustering a seismic catalog. In the seismological literature, the most used techniques can be divided into four big categories: window-based methods (e.g., Utsu, 1969; Knopoff and Gardner, 1972; Gardner and Knopoff, 1974; Keilis-Borok and

Kossobokov, 1986), link-based methods (e.g., Savage, 1972; Reasenberg, 1985; Frohlich and Davis, 1990; Davis and Frohlich, 1991) stochastic methods (e.g., Kagan and Jackson, 1991; Zhuang *et al*., 2002; Console *et al*., 2010a) and correlation metric methods (e.g., Baiesi and Paczuski, 2004; 2005; Zaliapin *et al*., 2008; Zaliapin and Ben- Zion, 2013a; 2013b).

These methods are mainly distinguished by the different models used to characterize the independent events. In detail, the window-based, the link-based and the correlation metric methods have a deterministic and dichotomic approach in the different attributes' selection, classifying an earthquake as either a mainshock or an aftershock or considering a-priori values for the parameters in the Gutenberg-Richter scaling law.

On the other hand, in the stochastic approaches, the background seismicity separation from the clustering components is executed starting from the attribution of probability for each event being triggered by another previous event or being an independent event. In the algorithm proposed for the first time by Zhuang *et al.* (2002), these probabilities are computed through the background intensity estimation, considered as a space function constant with time, and through the definitions of parameters associated with the clustered structures obtained by the epidemic-type aftershock sequence (ETAS) model. Although the choice of the best declustering approach is related to the specific pursued goals and to the catalog features (e.g., epicenter and source depth distributions, van Stiphout *et al.*, 2012), the stochastic methods present an approach that avoids subjective choices. Such objectivity makes these methods more reliable than the deterministic methods which assume arbitrary values for some declustering parameters definition, such as the space-time distance in which mainshocks act.

Moreover, as reported in the work of Mizrahi *et al*. (2021) the ETAS declustering processes appear to be the only declustering algorithms able to avoid bias in the *b*-value estimation for the declustered catalogs. The *b*-values are in fact strongly underestimated when the catalog declustering is executed

using window-based and link-based methods (e.g., Marzocchi and Taroni, 2014; Azak *et al*., 2018; Mizrahi *et al.*, 2021).

However, a correct and reliable seismicity rate and *b*-value estimation will be also related to the definition of the separation criterion to be used to attribute the different probabilities obtained by the stochastic declustering processes to the background and triggered contributes. Generally, in many studies these contributions are separated by choosing a threshold probability of independence (or triggered), with a purely subjective approach to the problem (e.g., Pintori *et al*., 2021). Instead, in other cases more complicated procedures have been shown: e.g., in the work of Ueda and Kato (2019) the background rate is obtained by averaging the different background rates built starting from a big number of stochastic declustered catalogs.

In this paper, we adopt an easier strategy for the definition of the independent and triggered seismicity rates, based on the sum of the probabilities for the seismic events to be independent or triggered, respectively. Such probabilities can also be used as weights to perform the *b*-value estimation for the background seismicity and for the clustered seismicity (Zhuang *et al*., 2004). So, by associating the weights obtained by the stochastic declustering with robust *b*-value estimation methods (Taroni *et al*. 2021b), it is possible to build *b*-value time series characterized by a high degree of reliability. For this work, we considered an Italian high resolution catalog of natural seismicity, recorded by the TABOO (The Alto Tiberina Near Fault Observatory) multidisciplinary research infrastructure managed by the Istituto Nazionale di Geofisica e Vulcanologia (INGV) (see “Dataset” section) (Chiaraluce *et al*., 2014). Starting from this catalog we have built seismicity rates and Gutenberg-Richter *b*-values time series using the declustering algorithm based on the ETAS-2D Model by Console *et al*. (2010b).

DATA

Dataset

TABOO is part of the community of the NFOs (Near Fault Observatories) that was built within the FP7 European project NERA – Network of European Research Infrastructures for Earthquake Risk Assessment and Mitigation (2010- 2014). This community presently consists of six multidisciplinary research infrastructures operating in regions characterized by high seismic hazard. NFOs are now part of the European Plate Observing System -Thematic Communities (Chiaraluce *et al*., 2022). NFOs collect multi- parametric near- fault data providing both raw data and advanced scientific products through the EPOS-related services. The TABOO target area is located along the upper Tiber Valley (northern Apennines of Italy, see Figure 1) where the Alto Tiberina Fault (ATF), an east-dipping low angle normal fault (dip 15°- 25°), dominates at depth an extensional fault system active in the Quaternary (Pialli *et al.*, 1998, Mirabella *et al*., 2011, Barchi *et al*., 1998, Boncio *et al*., 2000, Chiaraluce *et al*., 2014). This area perfectly fits the basic rules for being an NFO: it hosts active faults; it is relatively small; it is characterized by a relatively high seismicity. As this area was chosen as an NFO, the Italian National Seismic Network held by INGV was here progressively complemented with additional permanent seismic stations since January 2009, adjuvated by a short-term experiment (24 temporary stations were active between April 2010 and February 2011) and it was also progressively instrumented with several other multidisciplinary monitoring systems.

The INGV seismic network in the TABOO area before the NFO implantation consisted of 26 stations with minimum and median inter-distances of 6 km and 71 km, respectively (see Figure 1) while, excluding the temporary stations, it now consists of 55 stations with minimum and median inter-distances of 1 km and 50 km, respectively since 2010. Nevertheless, it is worth noting that the stations characterized by inter-distances as small as 10 to 30 km are prevalent within the network. This greatly improves the locations' quality, especially of the depth, keeping the closer station distance low. The

catalog used in the present paper was built by combining in a fully automatic work-flow (Di Stefano *et al*., 2014), a sensitive events detection, a high quality, P- and S-onset picking and weighting system (Di Stefano *et al.*, 2006; Aldersons *et al*., 2018), a local tomographic 3D velocity model built on purpose for the automatic workflow (Di Stefano *et al*., 2014) and a robust 3d tomographic and location code (SimulPS, Thurber, 1983; Ebenhart-Phillips, 1986; 1990). Finally, the resulting ~135k earthquakes where quality selected for RMS (≤ 0.3), number of phases (≥ 10), maximum GAP (≤ 270), maximum horizontal and vertical location errors (≤ 1.5km) and minimum number of stations with M_L estimation (≥ 5). The final dataset consists of ~50k high-quality located earthquakes from April 2010 to December 2015. M_L is calculated, for each event, as the median (with related standard deviation) over all the available stations' M_L. Stations' M_L are calculated by applying a derived attenuation law for the TABOO zone (Marzorati and Cattaneo, 2016) to the mean of the two horizontal channels' amplitude. Amplitudes in their turn are automatically estimated as the maximum peak-to-peak elongation of the signal after the convolution to standard Wood-Anderson sensor. A specificity of the applied method is the use of an adaptive band-pass pre-filtering. The algorithm automatically finds the optimum lower and upper corner frequency for the specific channel seismogram (sensor-earthquake couple) in the frequency range where signal to noise ratio is higher (over a given threshold of 5), so to better preserve also the signal of smaller magnitude events.

Maximum elongation is searched in a window extending from the automatic P-arrival, to 5s beyond the automatic/theoretical S-arrival time. The combination of the TABOO dense seismic network and the use of this adaptive filtering approach allowed a very low threshold in seismic event detection (M_L around 0.2) and a very low completeness magnitude of the catalog ($M_c = 0.5\ M_L$).

Catalog Analysis and Completeness magnitude estimation

The high-resolution TABOO catalog contains inside the volume (lat 42.6-44.2 *N*/lon 11.5-35.5 *E*) (-1.5<depth (km)< 34.16) 50,483 events from 1 st April 2010 up to 5 th December 2015, the last date on which the catalog was updated. TABOO catalog reports an abundance of small earthquakes that can help better characterize for this area the fundamental scaling laws of statistical seismology. The magnitude range starts from -2.77 M_L to a maximum magnitude equal to 4.01 obtained for the 28 th August 2010 earthquake with coordinates 12.670° *E* - 42.831° *N* at a depth of 7 km occurred 14 km south of Foligno (Perugia) **(**Figure 1**)**. The check of the quarry blasts inside the area by the catalog of non-tectonic earthquakes in Central-Eastern Italy, NTSEQS (Ladina *et al*. 2021) shows 191 artificial events that were removed from the dataset.

We focus our analysis inside the polygon, shown in Figure 1, which contains the major part of the seismicity along the Alto Tiberina low angle normal fault system (ATF) and Gubbio Fault (GF). In Table 1 the events with $M_L \geq 3.5$ are reported. The analysis of the events in depth shows that the major part of the seismicity is contained down to 15 km and as an additional check to be sure that we have deleted all the quarry blasts, we only analyze the dataset inside the depth range between 0.5 and 15.0 km.

One of the most important parameters for the statistical analysis of seismicity (and in particular the *b*-value) is the determination of the catalog's minimum completeness magnitude, *M*c. Different techniques have been suggested to estimate *M*c, like the Entire-magnitude-range method, the Maximum curvature-method, Goodness-of-fit test and *M*c by *b*-value stability (e.g., Ogata and Katsura, 1993; Rydelek and Sacks, 1989; Wiemer and Wyss, 2000; Cao and Gao, 2002).

We follow the approach suggested by Herrmann and Marzocchi (2021) as it is a conservative technique

to determine the *M*c of high-resolution earthquake catalogs. Consequently, we use the Lilliefors test (Lilliefors, 1969) as a statistical goodness-of-fit test with the exponential distribution to determine the lowest magnitude cut-off above which the magnitude is exponentially distributed. In other words, above $Mc^{Lilliefors}$, the frequency magnitude distribution (FMD) is consistent with the exponential-like Gutenberg–Richter relation. The *p*-value expresses the probability to observe the data sample assuming that the exponential distribution is true. We use a *p*-value with a significance level of $p = 0.1$, conservative in a statistical sense (Clauset *et al*., 2009) to obtain the lowest magnitude level above which the FMD can be considered exponential.

In Figure 2 the results of this analysis are reported. For our dataset (01/04/2010-05/12/2015) we obtain a $Mc^{Lilliefors} = 0.5$ with a total of 6531 events (0.5<depth (km) ≤15.0), which will be the dataset that we will use for subsequent analyzes. Further details about the completeness magnitude computation and its influence on the *b*-value estimation are reported in Supplemental Material-Texts S1 and S2 respectively.

METHODS

ETAS 2D model

The model applied in this study is based on the Epidemic Type Aftershock Sequence (ETAS) method and is used for an epicentral analysis (2D) of seismicity where depth has not been taken into account (ETAS 2D) (see e.g., Ogata, 1998 and 1999; Console and Murru, 2001; Console *et al*., 2003).

ETAS is a point process model which assumes that the earthquake sequence is made up of aftershocks and background events. Aftershocks include those events that are triggered by other earthquakes while background events are those that occur independent of other earthquakes. A few basic power laws, typical of complex systems are used: i) the Omori-Utsu (Utsu 1961, Ogata 1983) for the temporal

decay of the triggered events, and ii) the Utsu-Seki (Utsu and Seki, 1955) that describes the dependence of the number and spatial distribution of triggered earthquakes with the mainshock magnitude (see also Kanamori and Anderson, 1975).

One of the most remarkable features of such a model is that the magnitude of the triggered earthquakes is randomly sampled from a frequency-magnitude distribution, usually a Gutenberg-Richter law (Gutenberg and Richter, 1944). This implies no distinction between foreshocks, mainshocks, and aftershocks (e.g., Felzer *et al*., 2004) that can be identified only "a posteriori". In other words, there is no specific preparatory phase before a large earthquake because its probability is only proportional to the seismicity rate.

For the model, the expected number of earthquakes above M_{min} ($M_{min} \geq Mc^{\text{Lillieforse}}$) in the epicentral space-time unit window, given the observations before time t, at epicentral location $\vec{x}$ can be generically described as follows:

$$\lambda(t,\vec{x}) = \nu\mu(\vec{x}) + \sum_{i:t_i<t} \frac{k}{(t-t_i+c)^p}\left(\frac{(d_0 10^{\alpha(M_i-M_{min})})^2}{(d_0 10^{\alpha(M_i-M_{min})})^2 + |\vec{x}-\vec{x}_i|^2}\right)^q \quad [1]$$

Where:

- ν is a failure rate factor that represents the fraction of spontaneous events (i.e., the ratio between the expected number of independent events and the total number of events, ranging between 0 and 1);
- $\mu(\vec{x})$ represents the rate density of the long-term average seismicity;
- t_i defines the occurrence time of earthquakes;
- k is the productivity coefficient;
- c is the time constant of the Omori law;
- p is the exponent of the Omori law:

213 - q is the exponent of the epicentral spatial distribution of triggered events;

214 - d_0 is the epicentral characteristic triggering distance of an earthquake of magnitude M_{min};

215 - M_i is the magnitude of each earthquake considered;

216 - α is the coefficient of the exponential magnitude productivity law.

217 The epicentral smoothed total time-independent rate-density function $\mu(x)$ is computed using the
218 method introduced by Frankel (1995), described in detail by Console and Murru (2001) and Console
219 *et al.* (2003). The correlation distance used in the exponential kernel distribution of the smoothing
220 algorithm was found to be 4 km. It was determined by maximizing the likelihood of the seismicity in
221 half of the catalog under the time-independent model obtained from the other half and vice-versa.
222 The expression of the summation in equation [1] represents the triggering kernel that depends on time,
223 space, and magnitude. It considers the contribution of every previous event based upon the magnitude
224 of triggering events, the epicentral spatial distance of triggering earthquakes, and the time interval
225 between the triggering event and the forecast. This part is predominant during a sequence. The free
226 parameters of the model (k, c, p, q, d) are estimated by the maximum likelihood method. The
227 parameter ν is not determined from the best fit in the learning phase because it is related to all of the
228 other parameters of the model.
229 In the second step of the smoothing algorithm, the events receive a weight proportional to the
230 probability of being independent, with a number between 0 (if the event is totally triggered) and 1 (if
231 the event is totally independent) (Console *et al*., 2010a), as in the method introduced by Zhuang *et al*.
232 (2002). These weights were adjusted following an iterative procedure similar to that adopted by Marsan
233 and Longliné (2008). The final maximum-likelihood best-fit parameters of the ETAS model applied
234 to our data-set are shown in Table 2.
235

With this approach it is possible to assign to each event a weight equal to the probability to be independent without the need of removing events from the catalog.

Number of occurrences estimation in time

The strategy here used to separate the seismic occurrences for the different seismicity contributions is based on the probability of an event to be independent and its complementary value, estimated by the ETAS declustering process. In detail, in order to obtain the occurrence number of independent events (Sb_k) at the *k*-time window, we considered the sum of independence probabilities (φ_i) for each earthquake until the i_{th} event, as reported in equation [2]:

$$Sb_k = \sum_i \varphi_i \qquad [2]$$

In this way the independence probabilities acting as weights will allow us to compute the background occurrences simply by giving a different importance to the different earthquakes recorded in the catalog. The greater the independence probability of an event, the greater its weight in the estimation of background occurrences and vice versa.

Following the same approach and defying the triggered probability as:

$$\varrho_i = 1 - \varphi_i \qquad [3]$$

the occurrence number of clustered seismicity at the *k*-th window (Sc_k) will always be expressed as the sum of these probabilities:

$$Sc_k = \sum_i 1 - \varphi_i \quad [4]$$

This method which allows to quickly separate the number of occurrences of the different components of seismicity, appears simple from a mathematical point of view avoiding any type of subjectivism.

Fourier Transform

In this study, in order to analyze the periodical features of the independent seismicity rate in our dataset, we make use of the definition of the Fourier transform of a time function $f(t)$ as:

$$\Im[f(t)\ ] = F(\omega) = \int_{-\infty}^{+\infty} f(t)\ \ e^{-i\omega t}\, dt \quad [5]$$

where i is the imaginary unit.

We apply this definition to the function describing the time history of the seismicity rate by means of a computer code, performing the integral [5] by a numerical discretization. In order to obtain realistic results, an appropriate discretization has to be chosen for the input and output functions. As $F(\omega)$ is a complex number, we consider just its absolute value $|F(\omega)|$ in the presentation of our results.

Estimation of the *b*-value in time

The estimate of the changes in the *b*-value was performed by the "Weighted Likelihood Estimation" (WLE) approach (Taroni *et al*., 2021a). According to this method, the *b*-value estimate at time *t*, *b*(t), is performed considering all the events until the time *t*, and attributing to each of them a weight that varies according to the temporal distance with respect to time *t* (Eq. 4 in Taroni *et al*., 2021b). In this way, avoiding using a fixed number of events, as defined in the classic "Rolling Window Approach"

(e.g., Gulia and Wiemer, 2019), and therefore avoiding obtaining time windows of different lengths, it is possible to ensure that only the recent events may be relevant in the estimation of the *b*-value, thus obtaining a more robust and objective estimation of *b*-value changes over time. Here the WLE is used both to properly take into account the temporal variation of the seismicity and to correctly consider the weights assigned to each event by the stochastic declustering following Console *et al.* (2010a) technique. Indeed, in order to estimate the *b*-value contributions relating to background ($\hat{b}(t)_{back}$) and triggered ($\hat{b}(t)_{trig}$) seismicity, we implemented the WLE algorithm through additional weights as reported in the equations [6] and [7] respectively:

$$\hat{b}(t)_{back} = \frac{\sum_{i=1}^{n(t)} W(t_0 - t_i)\varphi_i}{ln(10)\left(\sum_{i=1}^{n(t)} W(t_0 - t_i)\varphi_i (M_i - M_c) + \frac{\Delta M}{2}\right)} \quad [6]$$

$$\hat{b}(t)_{trig} = \frac{\sum_{i=1}^{n(t)} W(t_0 - t_i)\varrho_i}{ln(10)\left(\sum_{i=1}^{n(t)} W(t_0 - t_i)\varrho_i (M_i - M_c) + \frac{\Delta M}{2}\right)} \quad [7]$$

Where $W(t_0 - t_i)\varphi_i$ and $W(t_0 - t_i)\varrho_i$ correspond to the weights assigned to each of the n(t) events considered up to time t; $W(t_0 - t_i)$ is the weight that depends on the time lapse between the i_{th} event and the first event in the catalog at time t_0, while the weights φ_i and ϱ_i are the ones related to the stochastic declustering algorithm, related to the background and triggering probability, respectively; M_i is the magnitude of the i_{th} event, ΔM is the magnitude binning, and M_c is the magnitude of completeness of the catalog. Then, using equations [6] and [7], it is possible to estimate the temporal variations of the *b*-value for the background and triggered events in the catalog, separately.

Such an approach also avoids the subjective choice of the number of events used for the temporal estimation of the *b*-value (usually 100 or 200 events, Taroni *et al*., 2021b). The importance of recent

289 events with respect to the earlier is controlled by the weight $W(t_0 - t_i)$, defined as $W(t_0 - t_i) =$
290 $exp(-\alpha \Delta T)$, where ΔT corresponds to time lapse between the i_{th} event and the first event in the
291 catalog, and α is the parameter that regulates the amount of past information relevant in the estimation
292 (this last parameter is objectively estimated with the maximum likelihood approach, as explained in
293 Taroni *et al*., 2021b). With respect to the equations of Taroni *et al*., 2021b, here we used non-
294 normalized weights, because our weights are composed by two different factors, then the numerator
295 of equations [6] and [7] is not equal to 1 but is equal to the sum of all the weights considered in the
296 computation.
297
298 **RESULTS**
299 In this section we present the time series both of seismic rate and Gutenberg-Richter *b*-value for the
300 TABOO catalog, starting from the ETAS 2D model, composed by 6,523 events recorded from 11 th
301 April 2010 to 5th December 2015. The earthquakes recorded from 1th to 10th April 2010 were not used
302 for this analysis due to the so-called "warm-up" phenomenon, consisting in an unrealistic high
303 probability of independence of the events in the initial part of the catalog, due to the omission of
304 previous triggering earthquakes. The ETAS model in fact associates an independence probability equal
305 to 1 to all those events without information on foreshocks. Therefore, in order to ensure data stability,
306 the first 10 days of the TABOO catalog have been removed.
307 For the seismic rate analysis, we considered not only the daily variation of the event number that
308 occurred in the whole TABOO catalog, but also the changes related to the background and triggered
309 components. As mentioned above, the separation of the different contributions was possible through
310 the independence probability values obtained from the ETAS declustering algorithm by Console *et al.*
311 (2010a). In detail, summing the independence probability (φ_i) (by eq.2) and the triggered probability

(ϱ_i) (by eq. 4), we have obtained the background and triggered daily seismic rates, respectively. The results of these computations are shown in Figure 3.

Observing the incremental and cumulative event number distribution in time we can note a twofold behaviour in the earthquake occurrence. The first part of the catalog, from April 2010 to about March 2013, is in fact characterized by a low number of events (about 1456) with an occurrence of about 1.4 earthquakes per day. Moreover, in this time lapse the number of background and triggered events (about 713 and 743, respectively) appears very similar.

Instead, in the last years, since March-April 2013 to December 2015, the seismicity rate increased sharply and a largest daily variation has been recorded, with the average occurrence of about 6.5 events per day in a small-time interval from March 2013 to October 2014 (seismic swarms). This earthquake frequency increase appears to be closely related to the triggered events whose number is equal to 4299 in the second part of the catalog, reaching a maximum value of about 3522 events during the year ranging between 2013-2014. On the other hand, though in the last few years the background seismicity is still characterized by a low number of earthquakes (about 772), also for this component the maximum number of occurrences results concentrated during the seismic swarms of 2013-2014, which mainly affected the municipalities of Città di Castello, Gubbio and Pietralunga.

The seismic background highlights small variations, which are better visible by analyzing the seismicity rate with a bigger observation window. In fact, observing the monthly behavior of the background (Figure 4a), the non-stationarity of this component appears evident, showing two maximum values, one at the beginning of 2011 and the other one in the second half of 2014.

This trend is clearly shown also with a quantitative approach through Fourier transform executed for the background events, where the maximum frequency is defined for a time period of about 40 months (peak at 0.025 in Figure 4b). Given the short duration of the recording of the seismic catalog (5 years) with respect to the oscillation period detected (40 months), whether such variations are linked to a real periodic behavior of the background or whether the maximum occurrence values are due to transient phenomena appears not simple to understand.

For the *b*-value analysis, as in the previous analysis, we consider the time series of the whole TABOO catalog and also the changes related to the background and triggered components separately. The results of the estimations are reported in Figure 5a, where the black, red and blue lines indicate the *b*-value time series for the whole catalog, for the background seismicity and for triggered events, respectively. These curves were built estimating forgetting parameter $\alpha = 0.020$ for our catalog. Further information about the *b*-values estimation errors in terms of standard deviations are available in the Supplemental Material-Text S3.

Observing the curves reported above, we can note that for the entire duration of the recording, the *b*-values estimated considering all the events of the TABOO catalog are ranging between the *b*-values of the background events (higher) and the *b*-values of the triggered events (lower). In particular, this gap between the different *b*-values appears to be very small in the first three years of the catalog, from April 2010 to about March-April 2013, where the *b*-average values are near to 1.1 both for the entire catalog and for the different components of the seismicity.

As clearly highlighted by the distribution of magnitude over time (Figure 5b), the number of events recorded in these first three years is very low, about 1/6 of that reported in the entire catalog. However, starting from April 2013, the different behavior between the *b*-values of background and *b*-values of triggered seismicity appears more evident. In fact, while for the background events the *b*-values

oscillate always around an average of about 1.1, for the triggered events the *b*-values show a sharp reduction reaching average values of about 0.8-0.9.

This different behavior of *b*-values estimated for the different components of seismicity is in line with the observations of Chiaraluce *et al*., 2007 and Valoroso *et al*., 2017, which mainly attribute this difference to the different structures responsible to generate independent events or triggered events. According to these authors, in fact, while the background seismicity is mostly attributable to the low-angle Alto-Tiberina fault (ATF), for which a number of events homogeneously distributed in time and space are evident, the triggering seismicity, characterized by multiple seismic sequences recorded mainly starting from April 2013 (Figure 5b), should instead be associated with the activity of the synthetic and antithetic faults placed on the ATF hanging wall.

Therefore, in the geological framework of the Alto-Tiberina fault system, the global *b*-value appears strongly affected by the triggered seismicity which is predominant in this study area, with a number of events equal to about 5042 out of a total number of 6523 events recorded. It is in progress a work that will examine the time and space variations of the seismicity rates and the Gutenberg-Richter *b*-values for the Alto Tiberina fault system, also taking in account the depths of events recorded in the TABOO catalog, through the construction of a new ETAS 3D model.

CONCLUSIONS

As demonstrated by numerous studies (e.g., Scholz 1968, 2015; Wiemer and Wyss, 1997; Wiemer *et al.*, 1998; Oncel and Wyss, 2000; Wyss *et al.*, 2001; Schorlemmer *et al.*, 2005; Murru *et al.*, 2005; Murru *et al.*, 2007; Meletti *et al.*, 2008; Bachmann *et al.*, 2012; Tormann *et al.*, 2014, 2015), *b*-values fluctuations could be related with physical proprieties and dynamism of the Earth crust. In particular, the recent work of Gulia and Weimer (2019) highlighted how the *b*-value temporal evolution could have a predictive meaning in the upcoming large-event occurrence. For these reasons, reliable

382 computation of the *b*- value time series represent an important instrument for a specific zone in the
383 seismic hazard assessment. Therefore, in this work, we wanted to present a series of procedures
384 finalized to an objective analysis of seismic catalogs to minimize biases in the *b*-value temporal
385 variation estimation for background and clustered seismicity. In detail, to separate the different
386 contributions of seismicity we proposed a new approach for the analysis of stochastic declustered
387 catalogs based on the use of weights obtained from the independence probabilities, achieved through
388 the construction of the ETAS 2D model. Thanks to our simple but rigorous approach that applies a
389 criterion not affected by subjective choices, the estimation of the seismic rates and Gutenberg-Richter
390 *b*-value time variations both for independence and triggered earthquakes is possible.
391 For demonstration purposes we applied this study to a high-resolution catalog. However, the
392 procedures shown can also be used for classical instrumental seismic catalog. In detail, this analysis
393 executed on TABOO catalog allowed to separate the background and clustered contributions for the
394 Alto-Tiberina seismic area, highlighting how the variations in the seismic rates and in the *b*-values are
395 mainly related to the triggered events that appear predominant in terms of number of occurrences in
396 the considered time period. Moreover, the seismic rate time series analysis puts in evidence the non-
397 stationarity for background seismicity, in which the biggest oscillations showed mostly a three-years
398 frequency. Regarding the *b*-value time series analysis, the estimations suggested a higher *b*-value for
399 background events with respect to triggered events.
400

401 **DATA AND RESOURCES**

402 The dataset considered in this work is generated by The Altotiberina Near Fault Observatory
403 (TABOO), an Istituto Nazionale di Geofisica e Vulcanologia monitoring infrastructure. This
404 infrastructure is part of the European Plate Observing System - Implementation Phase (EPOS-IP)

project, available at http://www.epos eu.org, which received funding from the European Union's Horizon 2020 research and innovation program under grant agreement 676564.

Query blasts analysis was executed considering the "Catalog of non-tectonic earthquakes in Central-Eastern Italy" redacted from the Ancona section of the INGV, available at http://www.an.ingv.it/NTSEQS

The *b*-value time series built through the "Weighted Likelihood Approach" were obtained using the code by Taroni *et al*. (2021) available at:

GitHub - MatteoTaroniINGV/Bvalue_TimeSeries_WeightedLikelihoodEstimation

All the graphs reported in the figures were made using Matlab codes

Figure 1 was made using Generic Mapping Tools (GMT) software (Wessel *et al.*,2013).

The Supplemental Material for this article includes further information about the reliability of *b*-value time series estimation. In particular, we focused on a) the magnitude of completeness estimation b) the influence of changes in completeness magnitude on the *b*-value time series and on c) the computation of *b*-values standard deviations.

ACKNOWLEDGEMENTS

This work was supported by the 2020-2023 INGV Department Strategic Project named MUSE Multiparametric and mUltiscale Study of Earthquake preparatory phase in the central and northern Apennines. We wish to thank the two reviewers for their valuable comments. We also thank the Editors of SRL for their support and encouragement.

REFERENCES

Aki, K. (1956). Some problems in statistical seismology, Zisin (Japanese) 8, 205-228. English translation by A. S. Furumoto, Univ. of Hawaii (1963). https://doi.org/10.4294/zisin1948.8.4_205

Aki, K. (1965). Maximum likelihood estimate of *b* in the formula logN=*a*-*b*M and its confidence limits. *Bull. Earthq. Res. Inst*. **43**, 237–239.

Alderson, D. L., Brown, G. G., Carlyle, W. M., Wood, R. K. (2018). Assessing and Improving the Operational Resilience of a Large Highway Infrastructure System to Worst-Case Losses. *Transp. Sci.* **52**(4), 1012-1034. https://doi.org/10.1287/trsc.2017.0749

Azak, T. E., Kalafat, D., Şeşetyan, K., and Demircioğlu, M. B. (2018). Effects of seismic declustering on seismic hazard assessment: a sensitivity study using the Turkish earthquake catalogue. *Bull. Earthquake Eng.*, **16**(8), 3339-3366. https://doi.org/10.1007/s10518-017-0174-y

Baiesi, M.,and Paczuski, M. (2004). Scale-free networks of earthquakes and aftershocks. *Physical review E*, **69**(6), 066106. https://doi.org/10.1103/PhysRevE.69.066106

Baiesi, M., and Paczuski, M. (2005). Complex networks of earthquakes and aftershocks. *Nonlin. Process. Geophys.*, **12**(1), 1-11. https://doi.org/10.5194/npg-12-1-2005

Bachmann, C., S. Wiemer, B. Goertz-Allmann, and Woessner, J. (2012), Influence of pore-pressure on the event-size distribution of induced earthquakes, *Geophys. Res. Lett.*, **39**, L09302. https://doi.org/10.1029/2012GL051480

Barchi, M. R., De Feyter, A., Magnani, M., Minelli, G., Pialli, G., and Sotera, B. M. (1998). Extensional tectonics in the Northern Apennines (Italy): Evidence from the CROP 03 deep seismic reflection line. *Mem. Soc. Geol. Ital.*, **52**, 528-538.

Boncio, P., Brozzetti, F., and Lavecchia, G. (2000). Architecture and seismotectonics of a regional low-angle normal fault zone in central Italy. *Tectonics*, **19**(6), 1038-1055. https://doi.org/10.1029/2000TC900023

Cao, A. M., and Gao, S. S. (2002). Temporal variations of seismic *b*-values beneath northeastern japan island arc. *Geophys. Res. Lett.*, **29**(9), 1334. https://doi.org/10.1029/2001GL013775

Chiaraluce, L., Chiarabba, C., Collettini, C., Piccinini, D., and Cocco, M. (2007). Architecture and mechanics of an active low angle normal fault: Alto Tiberina fault, northern Apennines, Italy. *J. Geophys Res: Solid Earth*, **112**(B10). https://doi.org/10.1029/2007JB005015

Chiaraluce L., A. Amato, S. Carannante, V. Castelli, M. Cattaneo, M. Cocco, C. Collettini, E. D'Alema, R. Di Stefano, D. Latorre, S. Marzorati, F. Mirabella, G. Monachesi, D. Piccinini, A. Nardi, A. Piersanti, S. Stramondo, L. Valoroso (2014). The Alto Tiberina Near Fault Observatory (northern Apennines, Italy). *Ann. Geophys.*, **57**(3), S0327. https://doi.org/10.4401/ag-6426

Chiaraluce, L., Festa, G., Bernard, P., Caracausi, A., Carluccio, I., Clinton, J., Di Stefano, R., Elia, L., Evangelidis, C.P., Ergintav, S., Jianu, O., Kaviris, G., Marmureanu, A., and Sokos, E. (2022). The Near Fault Observatory community in Europe: a new resource for faulting and hazard studies. *Ann. Geophys.*, **65**(3), DM316-DM316. https://doi:10.4401/ag-8778

Clauset, A., Shalizi, C. R., and Newman, M. E. (2009). Power-law distributions in empirical data. *SIAM review*, ***51***(4), 661-703. https://doi.org/10.48550/arXiv.0706.1062

Console, R., and Murru, M. (2001). A simple and testable model for earthquake clustering. *J. Geophys. Res.*: *Solid Earth*, **106**(B5), 8699-8711. https://doi.org/10.1029/2000JB900269

Console, R., Murru, M., and Lombardi, A. M. (2003). Refining earthquake clustering models. *J. Geophys. Res.*: *Solid Earth*, **108**(B10). https://doi.org/10.1029/2002JB002130

Console, R., Jackson, D. D., and Kagan, Y. Y. (2010a). Using the ETAS model for catalog declustering and seismic background assessment. *Pure Appl. Geophys.*, **167**(6), 819-830. https://doi.org/10.1007/s00024-010-0065-5

Console, R., Murru, M. and G. Falcone (2010b). Retrospective forecasting of M ≥ 4.0 earthquake in New Zealand, in Seismogenesis and Earthquake Forecasting: The Frank Evison Volume. *Pure Appl. Geophys.* https:// doi: 10.1007/s00024- 010-0068-2

Davis, S. D., and Frohlich, C. (1991). Single-link cluster analysis, synthetic earthquake catalogues, and aftershock identification. *Geophys. J. Int.*, **104**(2), 289-306. https://doi.org/10.1111/j.1365-246X.1991.tb02512.x

Di Stefano, R., Aldersons, F., Kissling, E., Baccheschi, P., Chiarabba, C., and Giardini, D. (2006). Automatic seismic phase picking and consistent observation error assessment: application to the Italian seismicity. *Geophys. J. Int.*, **165**(1), 121-134. https://doi.org/10.1111/j.1365-246X.2005.02799.x

Di Stefano, R., Chiaraluce, L., Valoroso, L., Waldhauser, F., Latorre, D., Piccinini, D., and Tinti, E. (2014, December). An automatic modular procedure to generate high-resolution earthquake catalogues: application to the Alto Tiberina Near Fault Observatory (TABOO), Italy. In *AGU Fall Meeting Abstracts* (Vol. 2014, pp. T13C-4684). https://doi.org/10.5281/zenodo.1222148

Eberhart-Phillips, D. (1986). Three-dimensional velocity structure in northern California Coast Ranges from inversion of local earthquake arrival times. *Bull. Seismol. Soc. Am.*, **76**(4), 1025-1052. https://doi.org/10.1785/BSSA0760041025

Eberhart- Phillips, D. (1990). Three - dimensional P and S velocity structure in the Coalinga region, California. *J. Geophys. Res.: Solid Earth*, **95**(B10), 15343-15363. https://doi.org/10.1029/JB095iB10p15343

Felzer, K.R., Abercrombie, R.E. and Ekstrom, G. (2004). A Common Origin of Aftershocks, Foreshocks, and Multiplets., *Bull. Seismol. Soc. Am.*, **94**, 88-98. https://doi.org/10.1.1.574.3527&

Frankel, A. (1995). Mapping seismic hazard in the central and eastern United States, *Seismol. Res. Lett.*, **66**, 8-21.

Gulia, L. and Wiemer, S. (2019). Real-time discrimination of earthquake foreshocks and aftershocks. *Nature*, **574**, 193–199. https://doi.org/10.1038/s41586-019-1606-4

Gutenberg, B. and C.F. Richter (1944). Frequency of earthquakes in California, *Bull. Seismol. Soc. Am.*, **34**, 185-188. http://dx.doi.org/10.1785/gssrl.66.4.8

Frohlich, C., and Davis, S. D. (1990). Single-link cluster analysis as a method to evaluate spatial and temporal properties of earthquake catalogues. *Geophys. J. Int.*, **100**(1), 19-32. https://doi.org/10.1111/j.1365-246X.1990.tb04564.x

Gardner, J. K., and Knopoff, L. (1974). Is the sequence of earthquakes in Southern California, with aftershocks removed, Poissonian? *Bull. Seismol. Soc. Am.*, **64**(5), 1363-1367. https://doi.org/10.1785/BSSA0640051363

Gutenberg, B., and Richter, C. F. (1944). Frequency of earthquakes in California. *Bull. Seismol. Soc. Am.*, **34**(4), 185-188. https://doi.org/10.1785/BSSA0340040185

Herrmann, M., and Marzocchi, W. (2021). Inconsistencies and lurking pitfalls in the magnitude–

frequency distribution of high - resolution earthquake catalogs. *Seismol. Res. Lett.*, **92**(2A), 909-922. https://doi.org/10.1785/0220200337

Kagan, Y. Y., and Jackson, D. D. (1991). Long-term earthquake clustering. *Geophys. J. Int.*, **104**(1), 117-133. https://doi.org/10.1111/j.1365-246X.1991.tb02498.x

Kanamori, H., Anderson, D. L. (1975). Theoretical basis of some empirical relations in seismology. *Bull. Seismol. Soc. Am.*, **65**(5), 1073-1095. https://doi.org/10.1785/BSSA0650051073

Keilis-Borok, V. I., and Kossobokov, V. G. (1986). Time of increased probability for the great earthquakes of the world. *Comput. Seismol.*, **19**, 48-58.

Knopoff, L. (1964). The statistics of earthquakes in Southern California. *Bull. Seismol. Soc. Am.*, **54**(6A), 1871-1873. https://doi.org/10.1785/BSSA05406A1871

Knopoff, L., and Gardner, J. K. (1972). Higher seismic activity during local night on the raw worldwide earthquake catalogue. *Geophys. J. Int.*, **28**(3), 311-313. https://doi.org/10.1111/j.1365-246X.1972.tb06133.x

Ladina C., Calamita C., Pantaleo D., Marzorati S., Cattaneo M., Frapiccini M., Monachesi G. (2021). NTSEQS: catalogue of non-tectonic earthquakes in Central-Eastern Italy, version 2.0 [Data set]. Istituto Nazionale di Geofisica e Vulcanologia (INGV). https://doi.org/10.13127/ntseqs2.0

Lilliefors, H. W. (1969). On the Kolmogorov-Smirnov test for the exponential distribution with mean unknown. *J. Am. Stat. Assoc.*, **64**(325), 387-389. https://doi.org/10.1080/01621459.1969.10500983

Marsan, D. and O. Longliné (2008). Extending earthquakes' reach through cascading, Science, **319**, 1076-1079. https://doi.org/10.1126/science.1148783

Marzocchi, W., and Taroni, M. (2014). Some thoughts on declustering in probabilistic seismic hazard analysis. *Bull. Seismol. Soc. Am.*, **104**(4), 1838-1845. https://doi.org/10.1785/0120130300

Marzorati, S., and Cattaneo, M. (2016). Stima automatica della magnitudo minima rilevabile dalla rete sismica ReSIICO. *Quaderni di Geofisica* **136**, 21.

Meletti, C., Galadini, F., Valensise, G., Stucchi, M., Basili, R., Barba, S., Vannucci, G. and Boschi, E. (2008). A seismic source zone model for the seismic hazard assessment of the Italian territory. *Tectonophysics*, **450**(1-4), 85-108. https://dx.doi.org/10.1016/j.tecto.2008.01.003

Mirabella, F., Brozzetti, F., Lupattelli, A., and Barchi, M. R. (2011). Tectonic evolution of a low angle extensional fault system from restored cross sections in the northern Apennines (Italy). *Tectonics*, **30**. https://doi.org/10.1029/2011TC002890

Mizrahi, L., S. Nandan, and S. Wiemer (2021). The Effect of Declustering on the Size Distribution of Mainshocks, *Seismol. Res. Lett.*, **92**, 2333-2342. https://doi: 10.1785/ 0220200231.

Murru, M., Montuori, C., Console, R., and Lisi, A. (2005). Mapping of the *b* value anomalies beneath Mt. Etna, Italy, during July–August 2001 lateral eruption. *Geophys. Res. Lett.*, **32**(5). https://doi.org/10.1029/2004GL021545

Murru, M., Console, R., Falcone, G., Montuori, C., and Sgroi, T. (2007). Spatial mapping of the *b* value at Mount Etna, Italy, using earthquake data recorded from 1999 to 2005. *J. Geophys. Res.: Solid Earth*, **112**(B12). https://doi.org/10.1029/2006JB004791

Ogata, Y. (1983). Estimation of the parameters in the modified Omori formula for aftershock frequencies by the maximum likelihood procedure. *J. Phys. Earth*, **31**(2), 115-124. https://doi.org/10.4294/jpe1952.31.115

549 Ogata, Y. (1998). Space-time point-process models for earthquake occurrences, *Ann. Inst. Statist.*
550 *Math.*, **50**(2), 379-402. https://doi.org/10.1023/A:1003403601725

551 Ogata, Y. (1999). Seismicity analysis through point-process modeling: A review, *Pure Appl. Geophys.*,
552 **155**, 471-507. https://doi.org/10.1007/s000240050275

553 Ogata, Y., and Katsura, K. (1993). Analysis of temporal and spatial heterogeneity of magnitude
554 frequency distribution inferred from earthquake catalogues. *Geophys. J. Int.*, **113**(3), 727-738.
555 https://doi.org/10.1111/j.1365-246X.1993.tb04663.x

556 Oncel, A., and Wyss, M. (2000). The major asperities of the 1999 Mw=7.4 Izmit earthquake defined
557 by the microseismicity of the two decades before it, *Geophys. J. Int.*, **143**, 501– 506.
558 https://doi.org/10.1046/j.1365-246X.2000.00211.x

559 Pialli, G., Barchi, M., and Minelli, G., editors. (1998). Results of the CROP03 deep seismic reflection
560 profile: *Mem. Soc. Geol. Ital.*, **52**, 647.

561 Pintori, F., Serpelloni, E., Longuevergne, L., Garcia, A., Faenza, L., D'Alberto, L., ... and Belardinelli,
562 M. E. (2021). Mechanical response of shallow crust to groundwater storage variations: Inferences from
563 deformation and seismic observations in the Eastern Southern Alps, Italy. *J. Geophys. Res.*: *Solid*
564 *Earth*, **126**(2). https://doi.org/10.1029/2020JB020586

565 Reasenberg, P. (1985). Second - order moment of central California seismicity, 1969–1982. *J.*
566 *Geophys. Res.*: *Solid Earth*, **90**(B7), 5479-5495. https://doi.org/10.1029/JB090iB07p05479

567 Rydelek, P. A., and Sacks, I. S. (1989). Testing the completeness of earthquake catalogues and the
568 hypothesis of self-similarity. *Nature*, **337**(6204), 251-253. https://doi.org/10.1038/337251a0

569 Savage, W. U. (1972). Microearthquake clustering near Fairview Peak, Nevada, and in the Nevada
570 seismic zone. *J. Geophys. Res.*, **77**(35), 7049-7056. https://doi.org/10.1029/JB077i035p07049

571 Scholz, C. H. (1968). The frequency magnitude relation of microfracturing in rock and its relation to
572 earthquakes, *Bull. Seismol. Soc. Am.*, **58** (1), 399–415. https://doi.org/10.1785/BSSA0580010399

573 Scholz C. H., (2015). On the stress dependence of the earthquake *b* value, *Geophys. Res. Lett.*, **42**,
574 1399–1402. https://doi.org/10.1002/2014GL062863

575 Schorlemmer, D., S. Wiemer, and Wyss, M. (2005). Variations in earthquake-size distribution across
576 different stress regimes, *Nature*, **437**, 539–542. https://doi.org/10.1038/nature04094

577 Taroni, M., Zhuang, J., and Marzocchi, W. (2021a). Highdefinition mapping of the Gutenberg–
578 Richter b- value and its relevance: A case study in Italy. *Seismol. Res. Lett.*, **92**(6), 3778-3784.
579 https://doi.org/10.1785/0220210017

580 Taroni, M., Vocalelli, G., and De Polis, A. (2021b). Gutenberg–Richter B-value time series
581 forecasting: A weighted likelihood approach. Forecasting, **3**(3), 561-569.
582 https://doi.org/10.3390/forecast3030035

583 Thurber, C. H. (1983). Earthquake locations and three - dimensional crustal structure in the Coyote
584 Lake area, central California. *J. Geophys Res: Solid Earth*, **88**(B10), 8226-8236.
585 http://dx.doi.org/10.1029/JB088iB10p08226

586 Tormann, T., B. Enescu, J. Woessner, and Wiemer, S. (2015). Randomness of megathrust earthquakes
587 implied by rapid stress recovery after the Japan earthquake, *Nature Geosci.*, **8** (2), 152–158.
588 https://doi.org/10.1038/ngeo2343

589 Tormann, T., S. Wiemer, and Mignan, A. (2014). Systematic survey of high-resolution b value imaging
590 along Californian faults: Inference on asperities, *J. Geophys. Res.*, **119 (**3), 2029–2054.
591 https://doi.org/10.1002/2013JB010867

592 Ueda, T., and Kato, A. (2019). Seasonal variations in crustal seismicity in San - in district, southwest
593 Japan. *Geophys. Res. Lett.*, **46**(6), 3172-3179.
594 https://doi.org/10.1029/2018GL081789

595 Utsu, T. (1961). A statistical study of the occurrence of aftershocks. *Geophys. Mag.*, **3**, 521-605.

596 Utsu, T. (1966). A statistical significance test of the difference in *b*-value between two earthquake
597 groups, *J. Phys. Earth.* **14**, 37–40.

598 Utsu, T. (1969). Aftershocks and earthquake statistics (1)-Some parameters which characterize an
599 aftershock sequence and their interrelations. *J. Fac. Hokkaido Univ.,* Ser. **7**, *3*, 125-195.

600 Utsu, T., and A. Seki (1955). Relation between the Area of the Aftershock Region and the Energy of
601 the Mainshock. *J. Seism. Soc. Japan*, **Ser II 7**, 233-240.

602 Valoroso, L., Chiaraluce, L., Di Stefano, R., and Monachesi, G. (2017). Mixed - mode slip behavior
603 of the Altotiberina low- angle normal fault system (Northern Apennines, Italy) through high-
604 resolution earthquake locations and repeating events. *J. Geophys. Res.: Solid Earth*, **122**(12), 10-220.
605 https://doi.org/10.1002/2017JB014607

606 van Stiphout, T., Zhuang, J., and Marsan, D. (2012). Seismicity declustering, *Community Online*
607 *Resour. Stat. Seism. Anal*. https://doi: 10.5078/corssa-52382934

Wessel, P. Smith, W. H., Scharroo, R., Luis, J., and F. Wobbe (2013). Generic mapping tools: improved version 528 released. *Eos Trans. AGU*, **94**(45), 409-410. https://doi.org/10.1002/2013EO450001

Wiemer, S., and Wyss, M. (1997). Mapping the frequency-magnitude distribution in asperities: An improved technique to calculate recurrence times?, *J. Geophys. Res*., **102,** 15115-15128. https://doi.org/10.1029/97JB00726

Wiemer, S. and Wyss, M. (2000). Minimum magnitude of completeness in earthquake catalogs: examples from Alaska, the Western United States, and Japan, *Bull. Seism. Soc. Am.*, **90**, 859-869. https://doi.org/10.1785/0119990114

Wiemer, S., S. McNutt, and Wyss, M. (1998). Temporal and three-dimensional spatial analyses of the frequency-magnitude distribution near Long Valley Caldera, California, *Geophys. J. Int.*, **134**, 409–421. https://doi.org/10.1046/j.1365-246x.1998.00561.x

Wyss, M., F. Klein, K. Nagamine, and Wiemer, S. (2001). Anomalously high *b*-values in the south flank of Kilauea Volcano, Hawaii: Evidence for the distribution of magma below Kilauea's east rift zone, *J. Volcanol. Geotherm. Res.*, **106**, 23–27. https://doi.org/10.1016/S0377-0273(00)00263-8

Zaliapin, I. A. Gabrielov, V. Keilis-Borok, and H. Wong (2008) Clustering Analysis of Seismicity and Aftershock Identification, *Phys. Rev. Lett.*, **101** (1), 1–4. https://doi.org/10.1103/PhysRevLett.101.018501

Zaliapin, I., and Ben- Zion, Y. (2013a) Earthquake clusters in southern California I: Identification and stability. *J. Geophys. Res.: Solid Earth*, **118**(6), 2847-2864. https://doi.org/10.1002/jgrb.50179

628 Zaliapin, I., & Ben- Zion, Y. (2013b). Earthquake clusters in southern California II: Classification and
629 relation to physical properties of the crust *J. Geophys. Res.: Solid Earth*, **118**(6), 2865-2877.
630 https://doi.org/10.1002/jgrb.50178Zhuang, J., Y. Ogata, and D. Vere-Jones (2002). Stochastic
631 declustering of space-time earthquake occurrences, *J. Am. Stat. Ass.*, **97** (458), 369-380, **102**(3), 1179-
632 1194.
633 https://doi.org/10.1198/016214502760046925

634 Zhuang, J., Ogata, Y., and Vere- Jones, D. (2004). Analyzing earthquake clustering features by using
635 stochastic reconstruction. *J. Geophys. Res.*: *Solid Earth*, **109**(B5).
636 https://doi.org/10.1029/2003JB002879

637

638 **Full mailing address for each author:**

639 Anna Eliana Pastoressa: Via di Vigna Murata 605, 00143, Rome, RM, Italy; email:
640 annaeliana.pastoressa@ingv.it

641 Maura Murru: Via di Vigna Murata 605, 00143, Rome, RM, Italy; email: maura.murru@ingv.it

642 Matteo Taroni: Via di Vigna Murata 605, 00143, Rome, RM, Italy; email: matteo.taroni@ingv.it

643 Rodolfo Console: Via di Vigna Murata 605, 00143, Rome, RM, Italy; email: rodolfo.console@ingv.it

644 Caterina Montuori: Via di Vigna Murata 605, 00143, Rome, RM, Italy; email:
645 caterina.montuori@ingv.it

646 Giuseppe Falcone: Via di Vigna Murata 605, 00143, Rome, RM, Italy; email:
647 giuseppe.falcone@ingv.it

Raffaele Di Stefano: Via di Vigna Murata 605, 00143, Rome, RM, Italy; email: raffaele.distefano@ingv.it

Tables:

Table 1. The strongest events with $M_L \geq 3.5$ in the area drawn from the polygon (Figure 1)

Province	Date (dd/mm/yyyy)	Latitude (degree)	Longitude (degree)	Local Magnitude (M_L)	Depth (km)
Pietralunga (PG)	15/04/2010	43.47	12.43	3.5	4.09
Gubbio (PG)	18/12/2013	43.38	12.52	3.6	3.18
Gubbio (PG)	22/12/2013	43.38	12.51	3.8	3.72

Table 2. Best-fit parameters of the ETAS 2D model optimized over the study period (1 April 2010–5 December 2015).

Parameter	Value
Number of events with $M \geq 2.1$	6,531
Lower magnitude threshold of triggering events	0.5
Lower magnitude threshold of target events	0.5
k (days $^{p-1}$) Productivity coefficient	5.34
c(days) Time constant in Omori law	0.02
q Exponent of the epicentral spatial distribution of triggered events	2.21
p Exponent in Omori law	1.16
d_0(km) Characteristic triggering distance in the spatial distribution	0.2
v Fraction of spontaneous events	0.23
$\ln L_1$ Maximum log-likelihood of the catalog under the clustering hypothesis	96,042.87
$\ln L_0$ Maximum log-likelihood of the catalog under the Poisson hypothesis.	64,127.69
$d\log L = \ln(L_1/L_0)$ Log-likelihood ratio	31,915.17

List of figure captions:

Figure 1. Epicentral distribution of all events falling within the TABOO area in the time period 1 April 2010 - 5 December 2015. The black polygon highlights the analyzed area. The ATF and GF are shown with red and yellow lines, respectively. The main municipalities are also indicated with yellow squares. The red and green triangles show permanent and temporary stations, respectively. The inset map shows the location in Italy of Figure 1.

Figure 2. Magnitude distribution for the TABOO catalog inside the polygon shown in Figure 1, for the time period 1 April 2010 - 5 December 2015. The left upper panel (a) shows the Lilliefors *p*-value as a function of *M*c, considering all the dataset magnitudes. The horizontal dashed line in red indicates

the significance level, 0.1, above which the FMD can be considered exponential. The right upper panel (b) the magnitude frequency distribution, considering all the dataset magnitudes. The red and blue dots indicate the exponential distribution and the cumulative number of events, respectively. The yellow vertical line indicates the considered $M_{c}^{\text{Lilliefors}}$. The bottom panel (c) is the sequential number of the events versus the magnitude from 1 to 6531, which corresponds to the first and last event of the dataset, respectively.

Figure 3. (a) Incremental number and (b) cumulative number of events daily recorded in the TABOO catalog from 11 April 2010 to 5 December 2015. The black, red and blue lines indicate the entire earthquake in the catalog, the independence and triggered events, respectively.

Figure 4. (a) Estimated number of background events occurred monthly (30 days); (b) frequency spectrum of the background seismicity computed through the Fourier Transform.

Figure 5. (a) *b*-value time series estimated using the weighted likelihood approach. The black line refers to all events recorded in the TABOO catalog, while the red line and the blue line are the *b*-values for background and clustered seismicity, respectively. (b) Magnitude earthquakes distribution over time.

Figures:

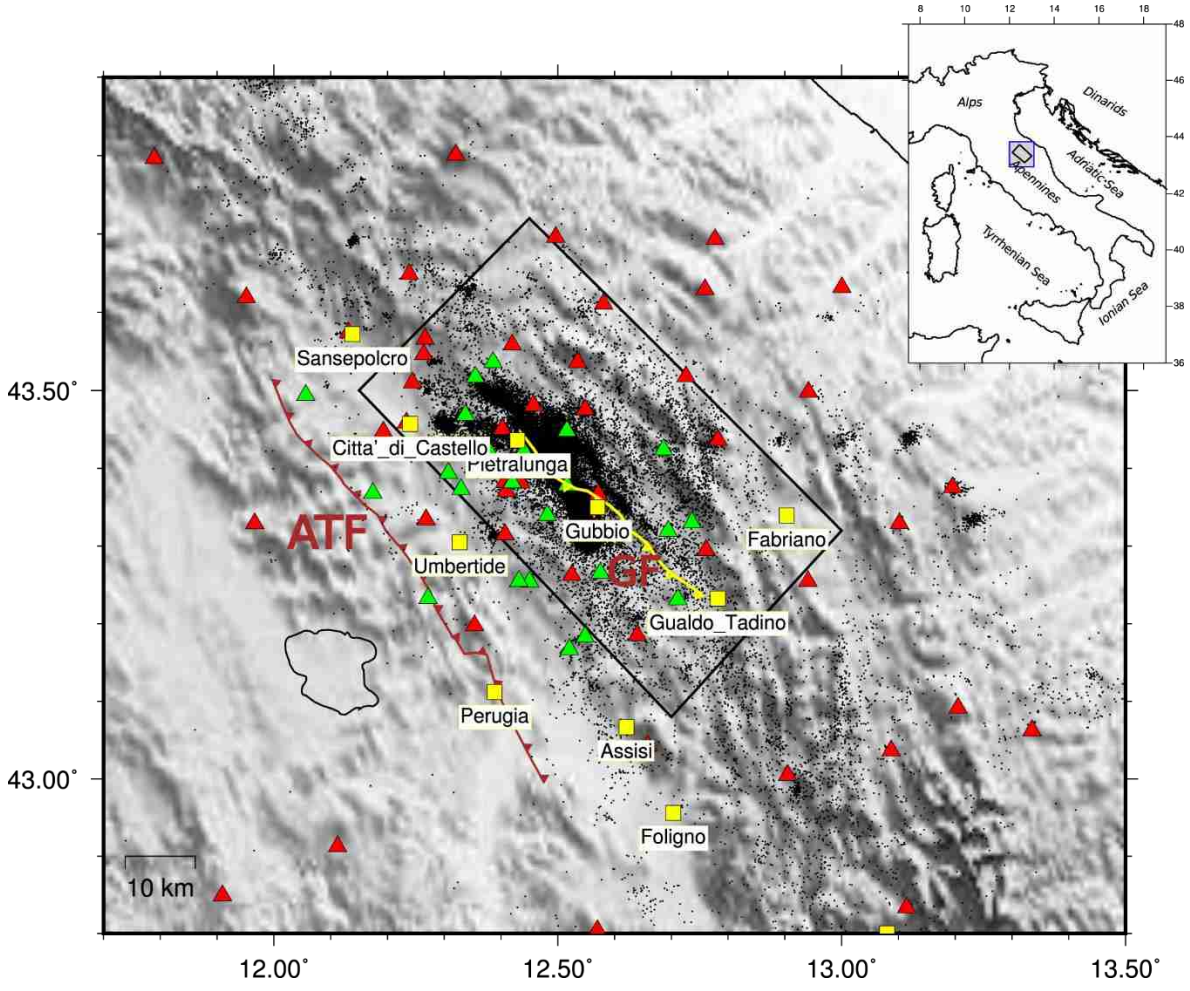

Figure 1. Epicentral distribution of all events falling within the TABOO area in the time period 1st April 2010 – 5th December 2015. The black polygon highlights the analyzed area. The ATF and GF are shown with red and yellow lines, respectively. The main municipalities are also indicated with yellow squares. The red and green triangles show permanent and temporary stations, respectively. The inset map shows the location in Italy of Figure 1. The color version of this figure is available only in the electronic edition.

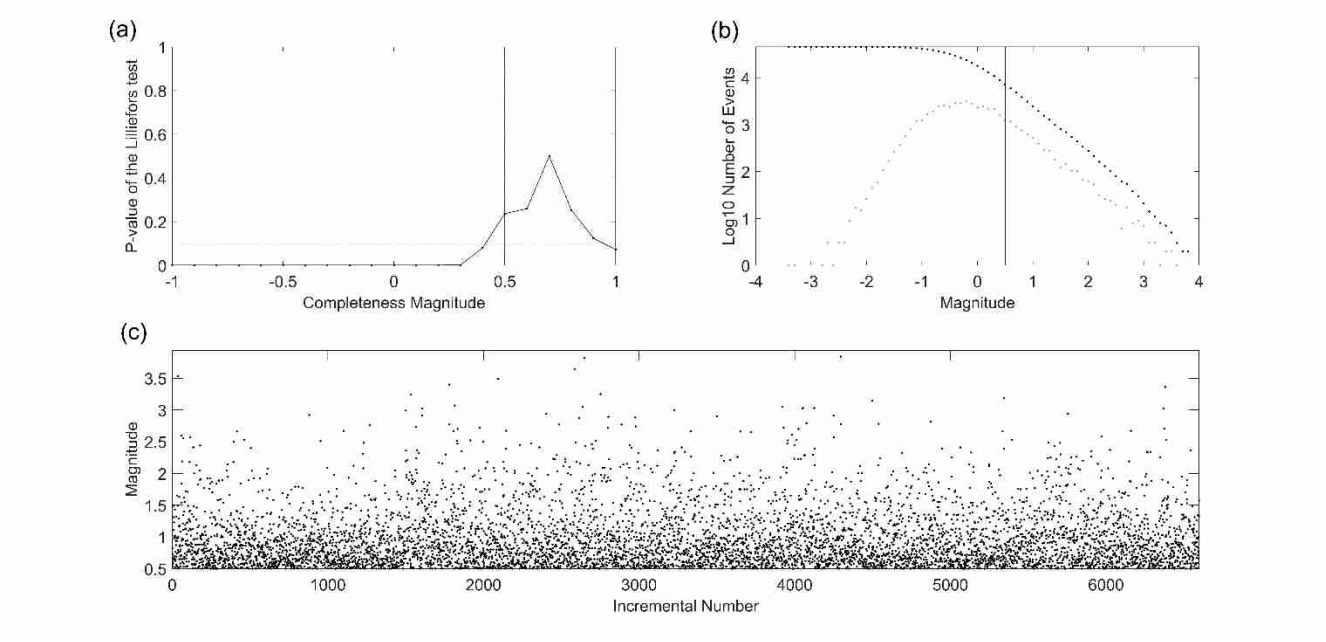

Figure 2. Magnitude distribution for the TABOO catalog inside the polygon shown in Figure 1, for the time period 1st April 2010 – 5th December 2015. The left upper panel (a) shows the Lilliefors *p*-value as a function of *M*c, considering all the dataset magnitudes. The horizontal dashed line indicates the significance level, 0.1, above which the FMD can be considered exponential. The right upper panel (b) the magnitude frequency distribution, considering all the dataset magnitudes. The grey and black dots indicate the exponential distribution and the cumulative number of events, respectively. The vertical line indicates the considered $Mc^{Lilliefors}$. The bottom panel (c) is the sequential number of the events versus the magnitude from 1 to 6·531, which corresponds to the first and last event of the dataset, respectively.

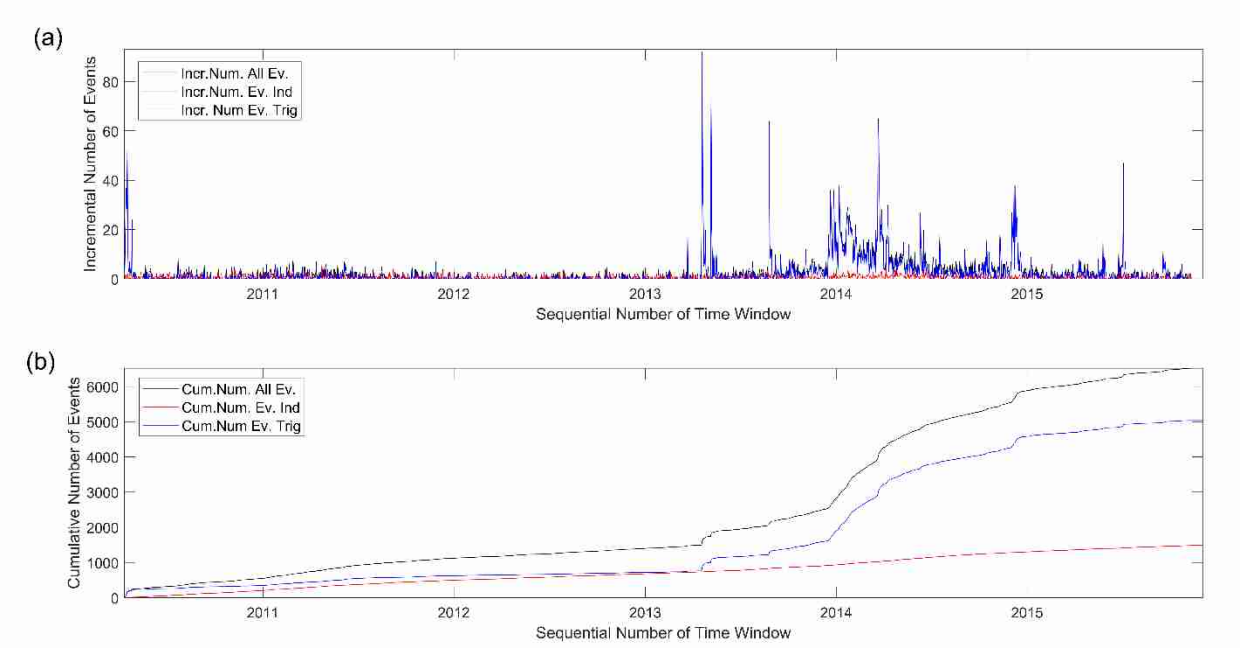

713

714 **Figure 3.** (a) Incremental number and (b) cumulative number of events daily recorded in the

715 TABOO catalog from 11th April 2010 to 5th December 2015. The black, red and blue lines indicate

716 the entire earthquake in the catalog, the independence and triggered events, respectively. The color

717 version of this figure is available only in the electronic edition.

718

719

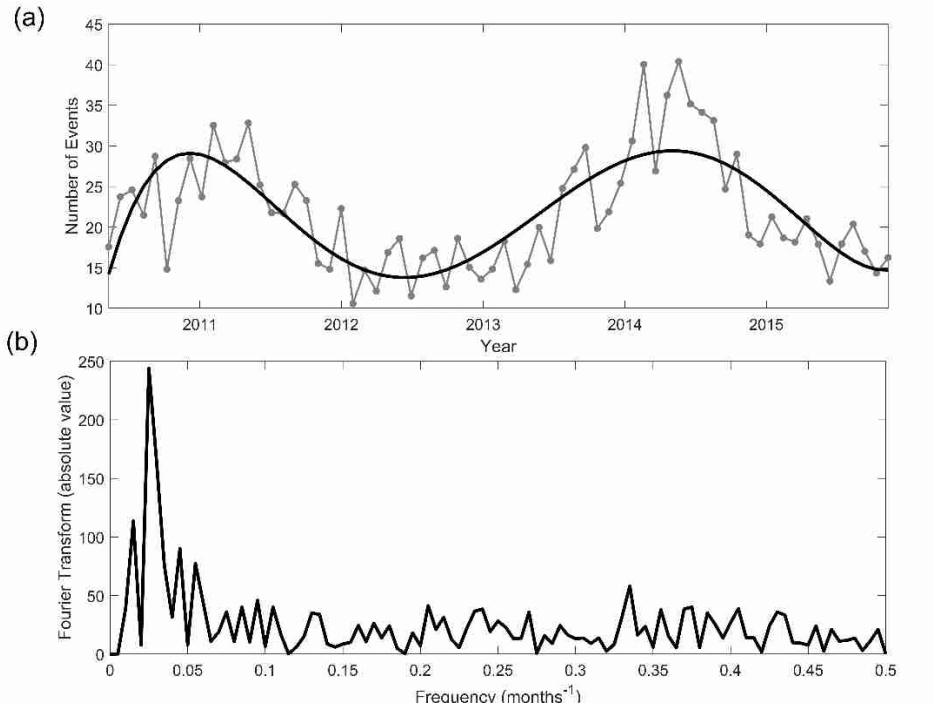

720

721 **Figure 4.** (a) Estimated number of background events occurred monthly (30 days); (b) frequency

722 spectrum of the background seismicity computed through the Fourier Transform.

723

724

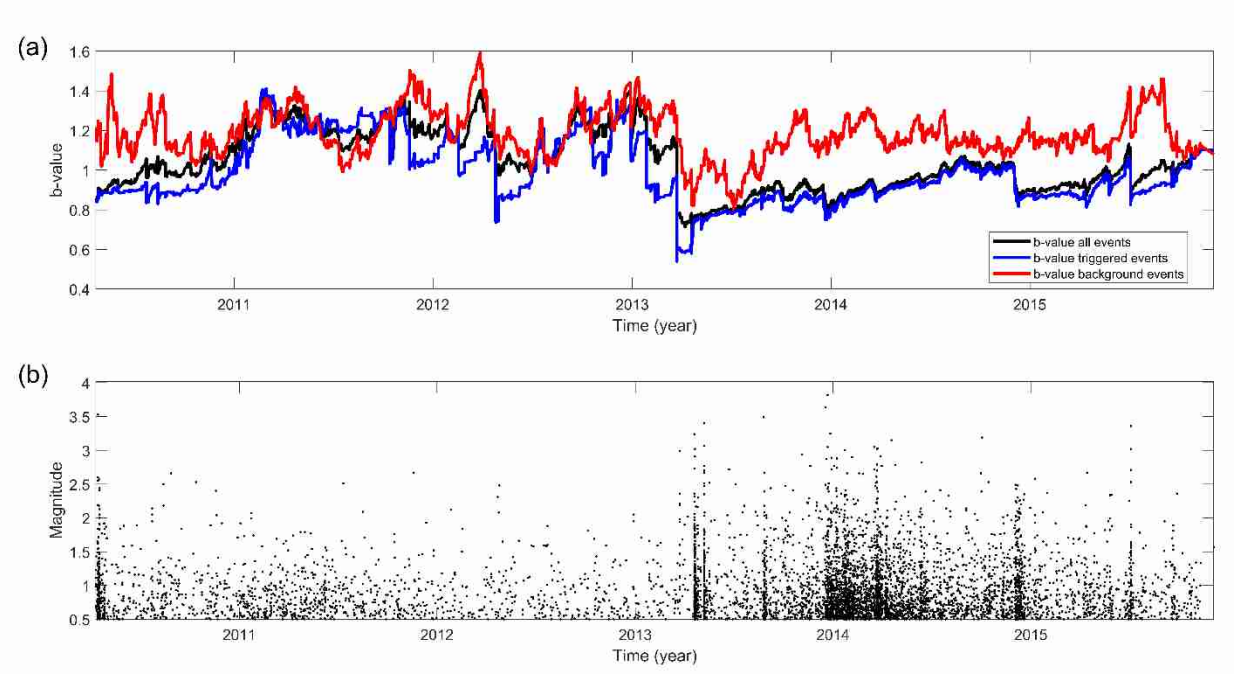

725

726 **Figure 5.** (a) *b*-value time series estimated using the weighted likelihood approach. The black line
727 refers to all events recorded in the TABOO catalog, while the red line and the blue line are the *b*-
728 values for background and clustered seismicity, respectively. (b) Magnitude earthquakes distribution
729 over time. The color version of this figure is available only in the electronic edition.

Figure 1

Click here to a

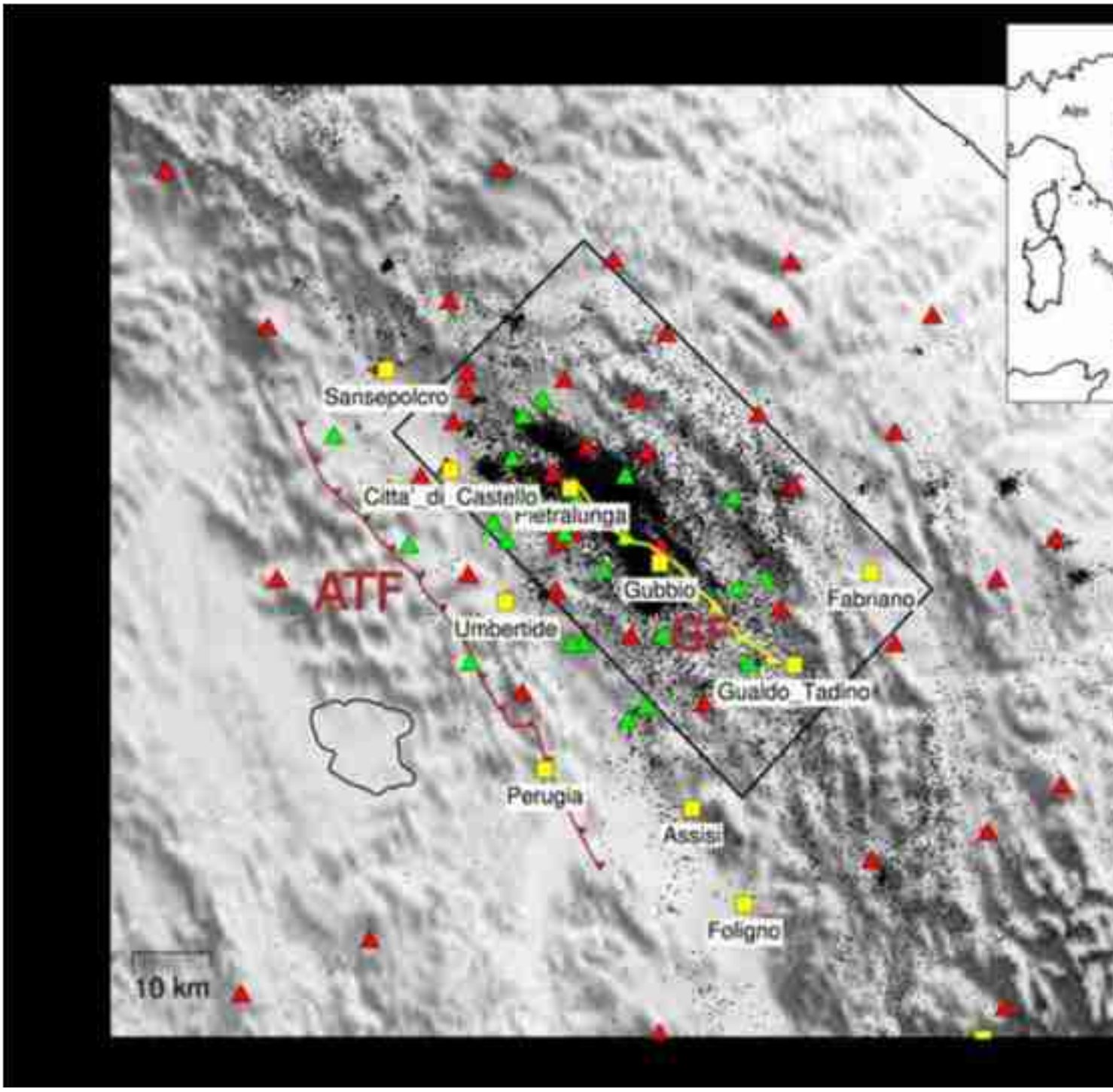

Figure 2

Click here to a

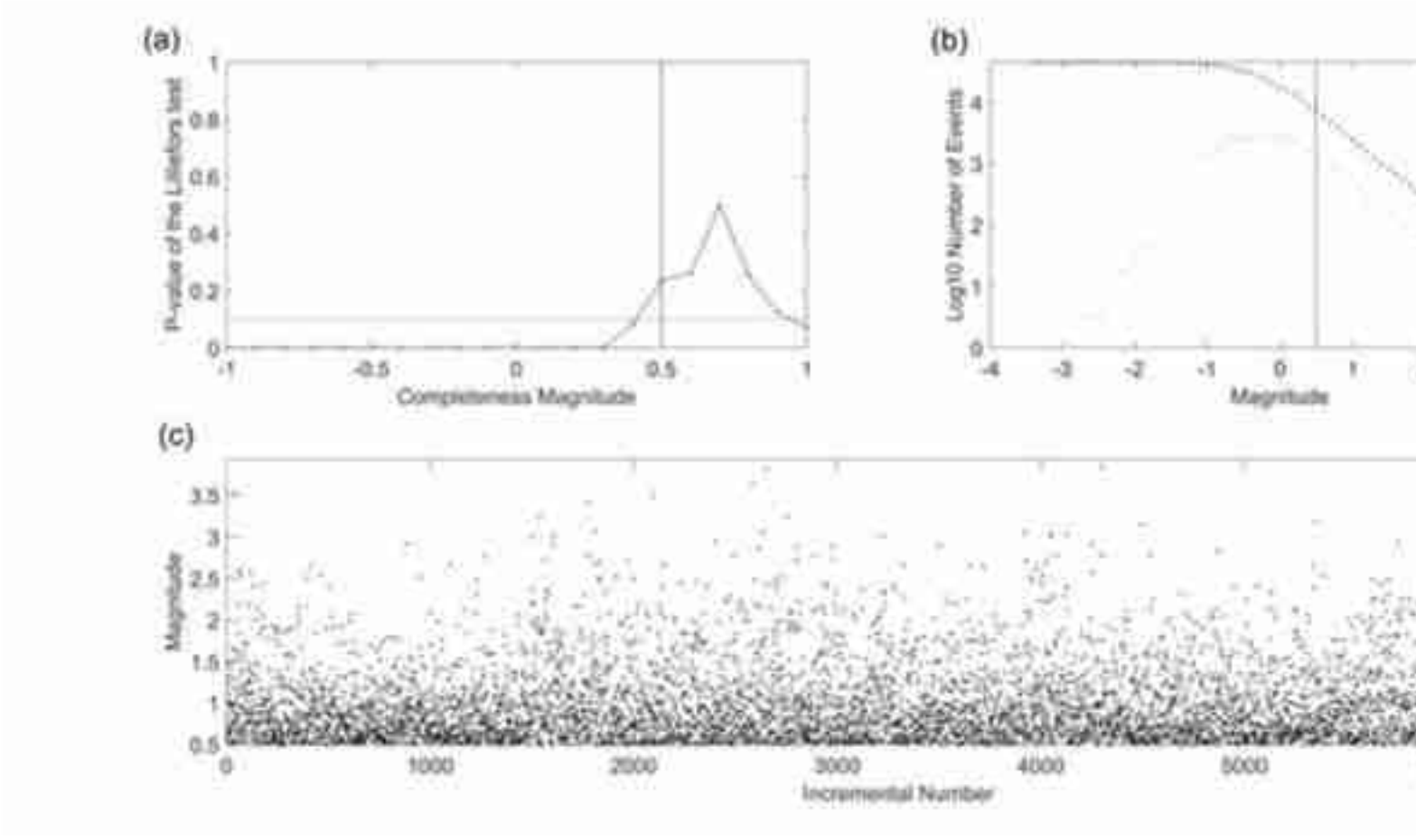

Figure 3

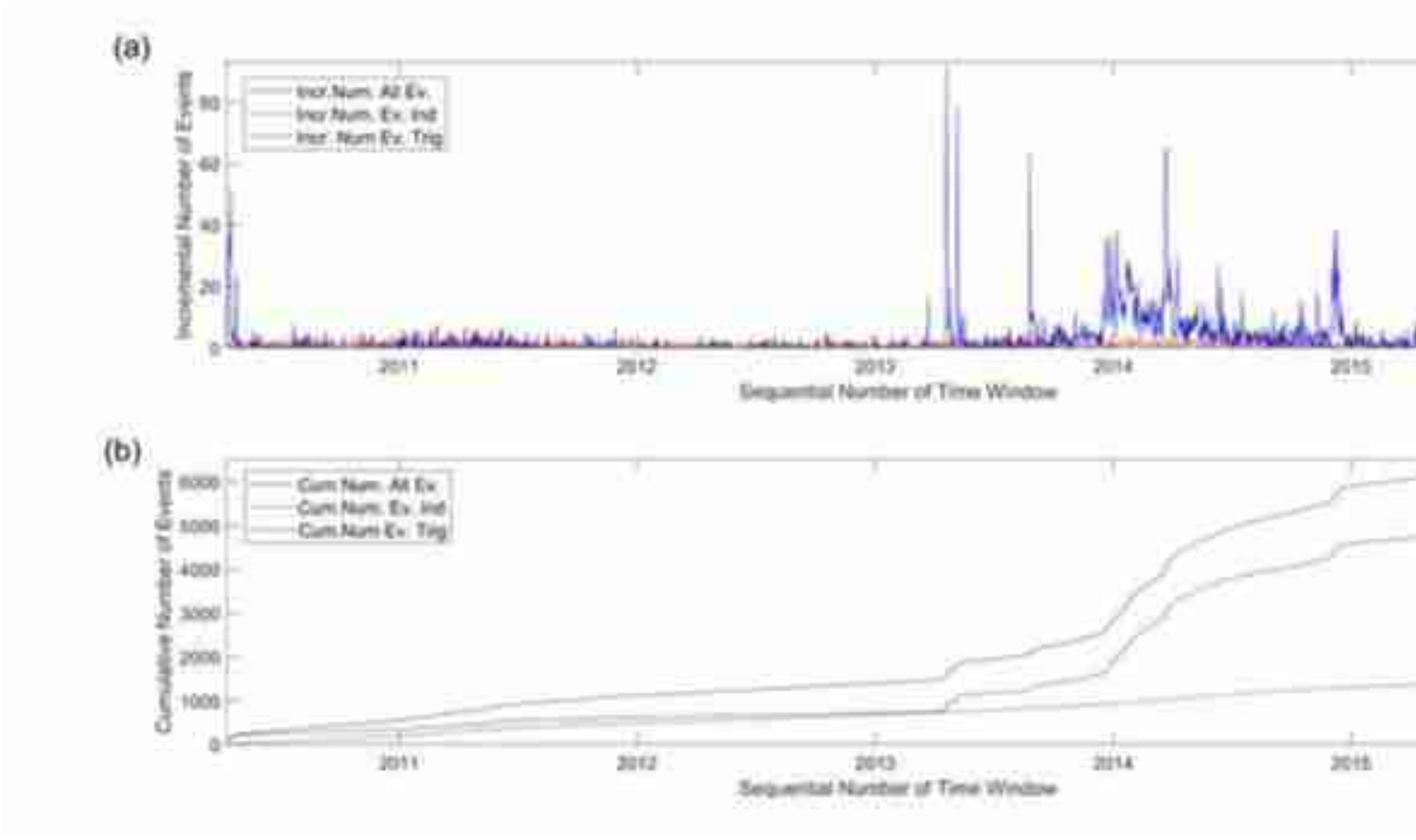
(a)
Incr.Num. All Ev.
Incr.Num. Ev. Ind
Incr. Num Ev. Trig
Incremental Number of Events
0
20
40
60
80
2011
2012
2013
2014
2015
Sequential Number of Time Window
(b)
Cum.Num. All Ev.
Cum.Num. Ev. Ind
Cum.Num Ev. Trig
Cumulative Number of Events
0
1000
2000
3000
4000
5000
6000
2011
2012
2013
2014
2015
Sequential Number of Time Window

Figure 4

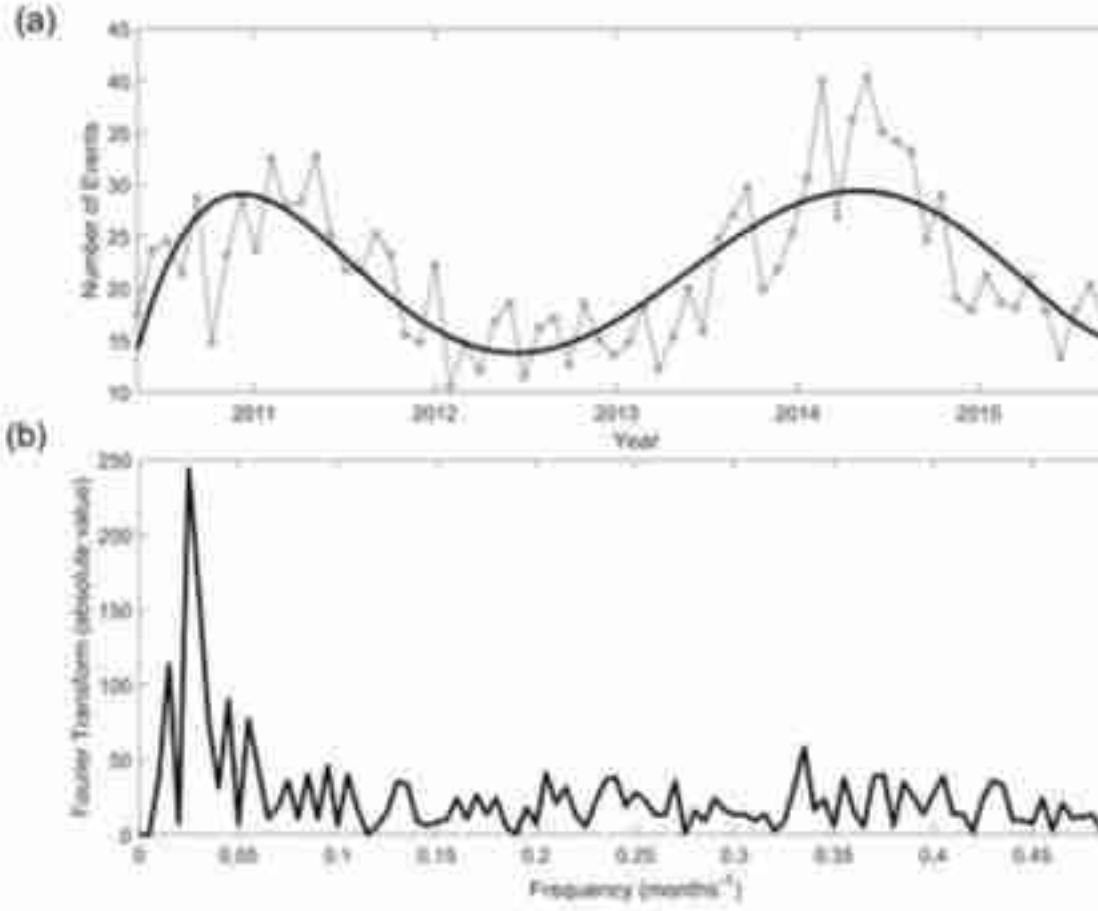

Figure 5

Click here to a

Temporal variations of seismicity rates and Gutenberg-Richter *b*-values for a stochastic declustered catalog: an example in central Italy

Anna Eliana Pastoressa, Maura Murru, Matteo Taroni, Rodolfo Console, Caterina Montuori, Giuseppe Falcone, Raffaele Di Stefano

Description of the Supplemental Material

In this document we report further information about the reliability of *b*-value time series estimation. In particular, we show a detailed description of approaches and procedures used to define the magnitude of completeness, also analysing *b*-value robustness with respect to completeness variation. Finally, in the last section, information about the computation and meaning of *b*-value standard deviation is reported.

Text S1

Magnitude of completeness estimation

In this work we performed a detailed magnitude of completeness estimation. We used one of the most conservative methods to compute the magnitude of completeness, i.e., the method suggested by Herrmann and Marzocchi (2021), based on the Lilliefors test (Lilliefors, 1969). Furthermore, we also investigated the so-called Short Term Aftershock Incompleteness (STAI), i.e. the temporal incompleteness that can affect seismic catalogs after the strongest events (Lolli and Gasperini, 2006). To deal with this problem, we applied the method proposed by Zhuang *et al*. (2017): this method consists in plotting the incremental number of events vs magnitude. In the case of STAI, in the lower part of the plot some empty spaces will appear (see e.g. Figure 2 of Zhuang *et al.* 2017). In our Figure 2c of the manuscript, there are no empty spaces in the lower part of the plot: then we can assert that

the estimated magnitude of completeness $Mc^{Lilliefors}$ = 0.5 is not affected by STAI, and it can be considered a reliable magnitude of completeness for the entire duration of the catalog.

Text S2

Influence of changes in completeness magnitude on the *b*-value estimation

Here we show the estimation of the *b*-value temporal variations with two conservative thresholds for the magnitude of completeness: 0.75 and 1.00. The results obtained are coherent with the ones relative to the magnitude of completeness of 0.5.

Text S3

Computation and meaning of the *b*-value estimation errors

In this section we show the *b*-value time series of TABOO catalog and their related estimation errors, expressed in terms of standard deviation, referring both to the entire catalog and to the background and clustered seismicity components **(**Figure S3**)**. The "Weighted Likelihood Method" proposed by Taroni *et al*. (2021a) allows in fact to estimate the *b*-value with the respective estimation errors (eq. 5 in Taroni *et al*. 2021b, using the weighting scheme defined in the "Estimation of the *b*-value in time" subsection within our manuscript).

In detail, the errors associated to the *b*-values of both the entire catalog and the two components of seismicity have average value of about ± 0.12 for the first three years of registration analyzed, while it tends to decrease around average value of about ± 0.04 for the entire catalog and for the triggered earthquakes in recent years recorded (from about March-April 2013 to December 2015).

The highest errors estimated for the first part of the catalog could be attributable to the lower number of events recorded in these first years, when a number of earthquakes equal to about 1/6 of those present in the whole catalog occurred. Therefore, also the largest *b*-values fluctuations found in this observation period can be attributed to stochastic variations linked to the little amount of data. Starting from the second half of 2013, with the increase in the earthquake occurrences mostly due to the increase of the number of the triggered events, the standard deviations for clustered and global seismicity decrease, while the *b*-value errors for the background show same values in time, probably attributable to the no significant variations in the number of events associated with it.

DATA AND RESOURCES

The dataset considered in this work is generated by The Altotiberina Near Fault Observatory (TABOO), an Istituto Nazionale di Geofisica e Vulcanologia monitoring infrastructure. This infrastructure is part of the European Plate Observing System - Implementation Phase (EPOS-IP) project, available at http://www.epos - eu.org, which received funding from the European Union's Horizon 2020 research and innovation program under grant agreement 676564.

The *b*-value time series built through the "Weighted Likelihood Approach" were obtained using the code by Taroni *et al*. (2021) available at:
GitHub - MatteoTaroniINGV/Bvalue_TimeSeries_WeightedLikelihoodEstimation

All the graphs reported in the figures were made using Matlab codes

REFERENCES FOR THE SUPPLEMENTARY MATERIAL

Herrmann, M., and Marzocchi, W. (2021). Inconsistencies and lurking pitfalls in the magnitude–frequency distribution of high- resolution earthquake catalogs. *Seismol. Res. Lett.*, **92**(2A), 909-922.

https://doi.org/10.1785/0220200337

Lilliefors, H. W. (1969). On the Kolmogorov-Smirnov test for the exponential distribution with mean unknown. *J. Am. Stat. Assoc.*, **64**(325), 387-389. https://doi.org/10.1080/01621459.1969.10500983

Lolli, B., and Gasperini, P. (2006). Comparing different models of aftershock rate decay: The role of catalog incompleteness in the first times after main shock. *Tectonophysics*, **423**(1-4), 43-59. https://doi.org/10.1016/j.tecto.2006.03.025

Taroni, M., Zhuang, J., and Marzocchi, W. (2021a). High - definition mapping of the Gutenberg–Richter b- value and its relevance: A case study in Italy. *Seismol. Res. Lett.*, **92**(6), 3778-3784. https://doi.org/10.1785/0220210017

Taroni, M., Vocalelli, G., and De Polis, A. (2021b). Gutenberg–Richter B-value time series forecasting: A weighted likelihood approach. Forecasting, **3**(3), 561-569. https://doi.org/10.3390/forecast3030035

Zhuang, J., Ogata, Y., and Wang, T. (2017). Data completeness of the Kumamoto earthquake sequence in the JMA catalog and its influence on the estimation of the ETAS parameters. *Earth, Planets and Space*, **69**(1), 1-12. https://doi.org/10.1186/s40623-017-0614-6

List of Supplemental Figure Captions

Figure S1. (a) *b*-value time series estimated using the weighted likelihood approach considering a magnitude of completeness equal to 0.75. The black line refers to all events recorded in the TABOO catalog, while the red line and the blue line are the *b*-values for background and clustered seismicity, respectively. (b) Magnitude earthquakes distribution over time.

Figure S2. (a) *b*-value time series estimated using the weighted likelihood approach considering a magnitude of completeness equal to 1. The black line refers to all events recorded in the TABOO catalog, while the red line and the blue line are the *b*-values for background and clustered seismicity, respectively. (b) Magnitude earthquakes distribution over time.

Figure S3. (a) *b*-value time series estimated using the weighted likelihood approach considering a magnitude of completeness equal to 0.5. The black line refers to all events recorded in the TABOO catalog, while the red line and the blue line are the *b*-values for background and clustered seismicity, respectively. The *b*-value standard deviation for the entire catalog is indicated by the dashed line while the standard deviations for independent and triggered events are represented by red and blue dashed lines, respectively. (b) Magnitude earthquakes distribution over time.

Figures:

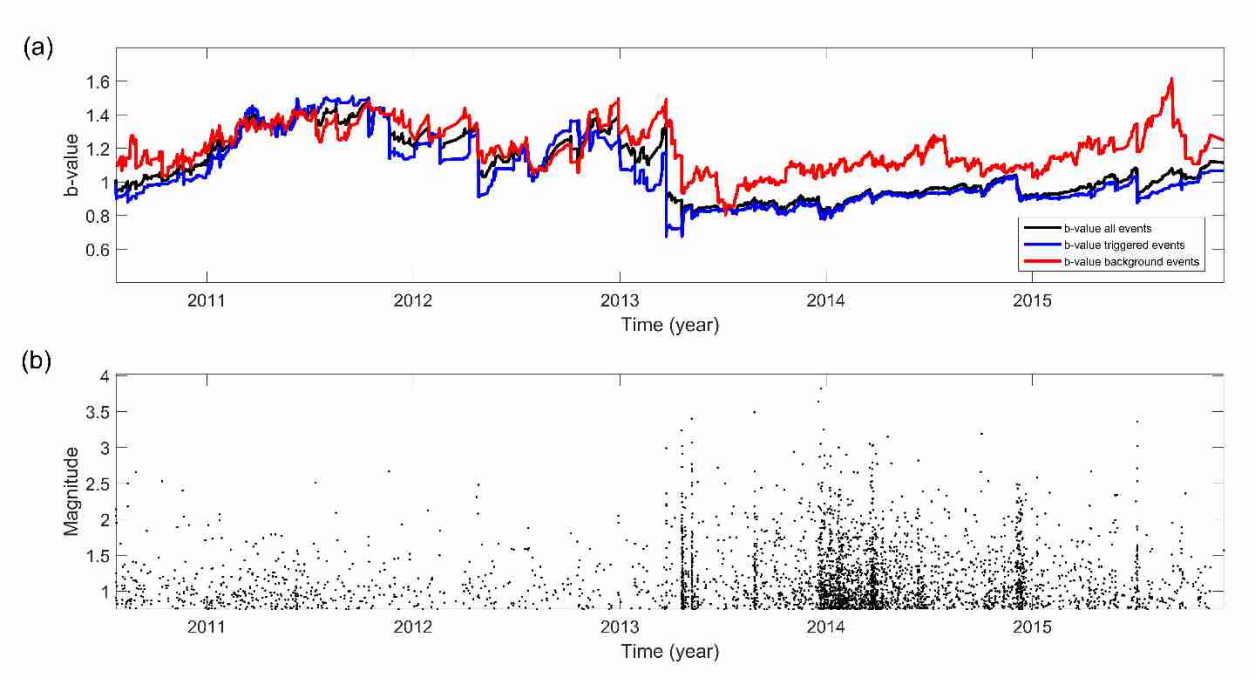

Figure S1. (a) *b*-value time series estimated using the weighted likelihood approach considering a magnitude of completeness equal to 0.75. The black line refers to all events recorded in the TABOO

catalog, while the red line and the blue line are the *b*-values for background and clustered seismicity, respectively. (b) Magnitude earthquakes distribution over time.

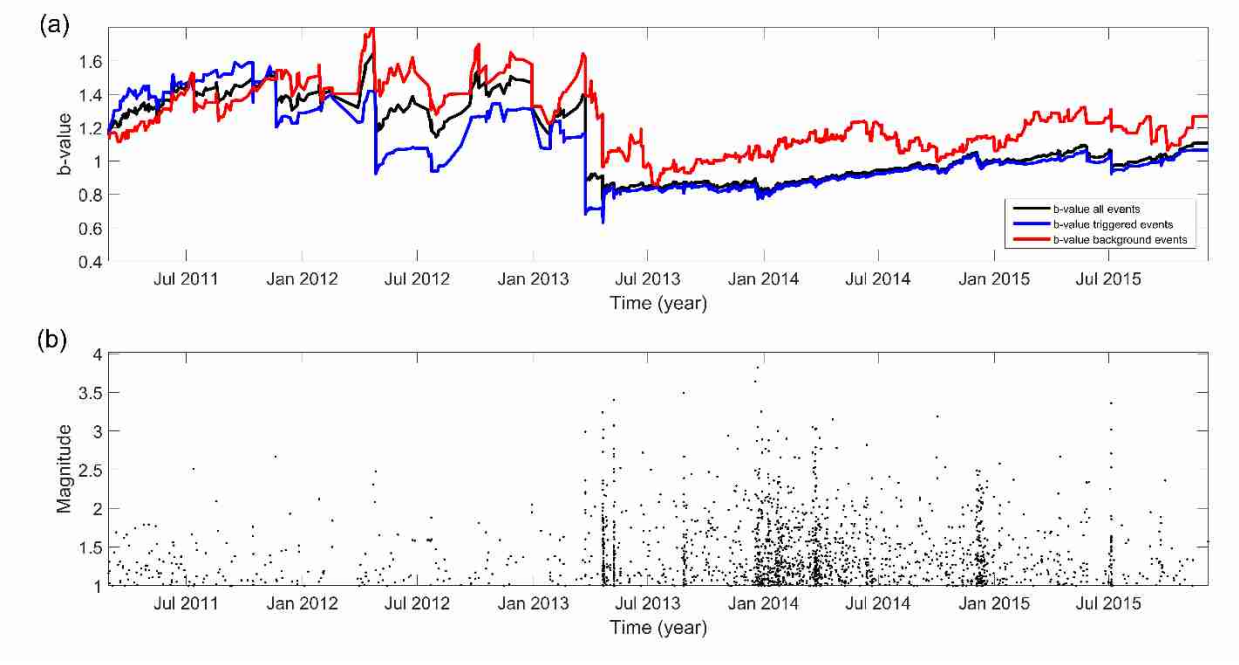

Figure S2. (a) *b*-value time series estimated using the weighted likelihood approach considering a magnitude of completeness equal to 1. The black line refers to all events recorded in the TABOO catalog, while the red line and the blue line are the *b*-values for background and clustered seismicity, respectively. (b) Magnitude earthquakes distribution over time.

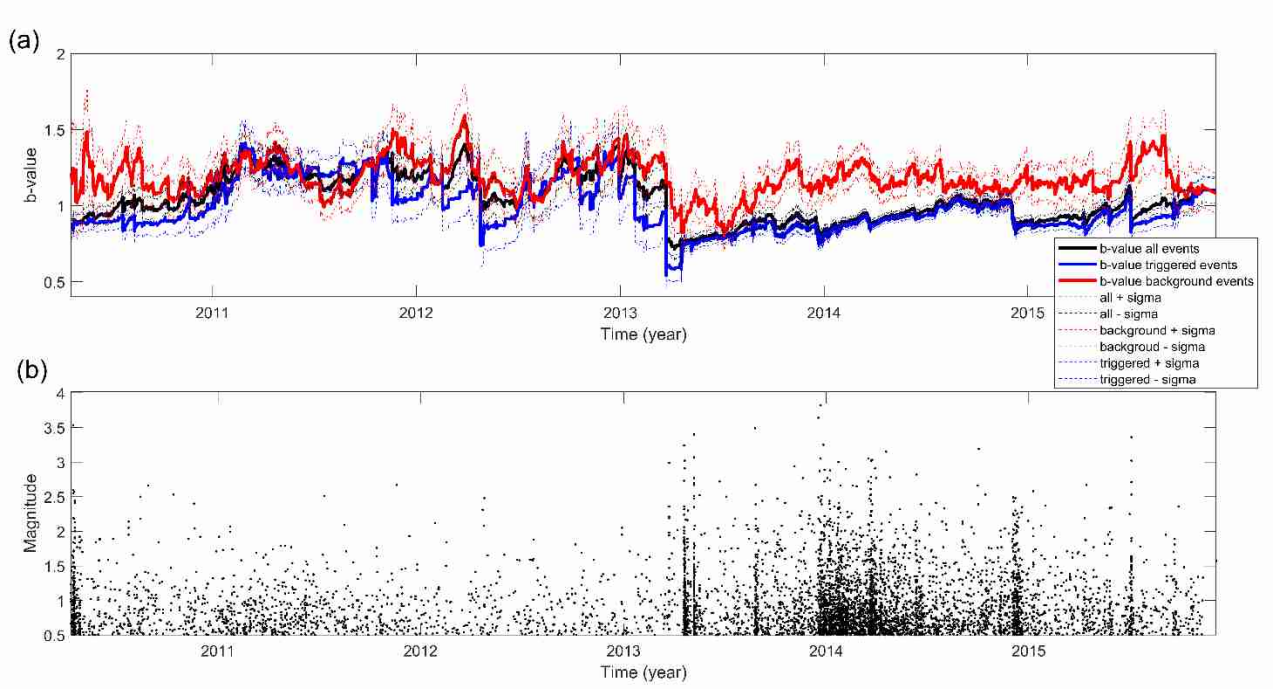

117

118 **Figure S3**. (a) *b*-value time series estimated using the Weighted Likelihood Approach. The black
119 line refers to all events recorded in the TABOO catalog, while the red line and the blue line are the
120 *b*-values for background and clustered seismicity, respectively. The *b*-value standard deviation for
121 the entire catalog is indicated by the dot line while the standard deviations for independent and
122 triggered events are represented by red and blue dot lines, respectively. (b) Magnitude earthquakes
123 distribution over time.

124

Figure S1

Click here to access/download;Supplemental Figures);FigureS1.jpg

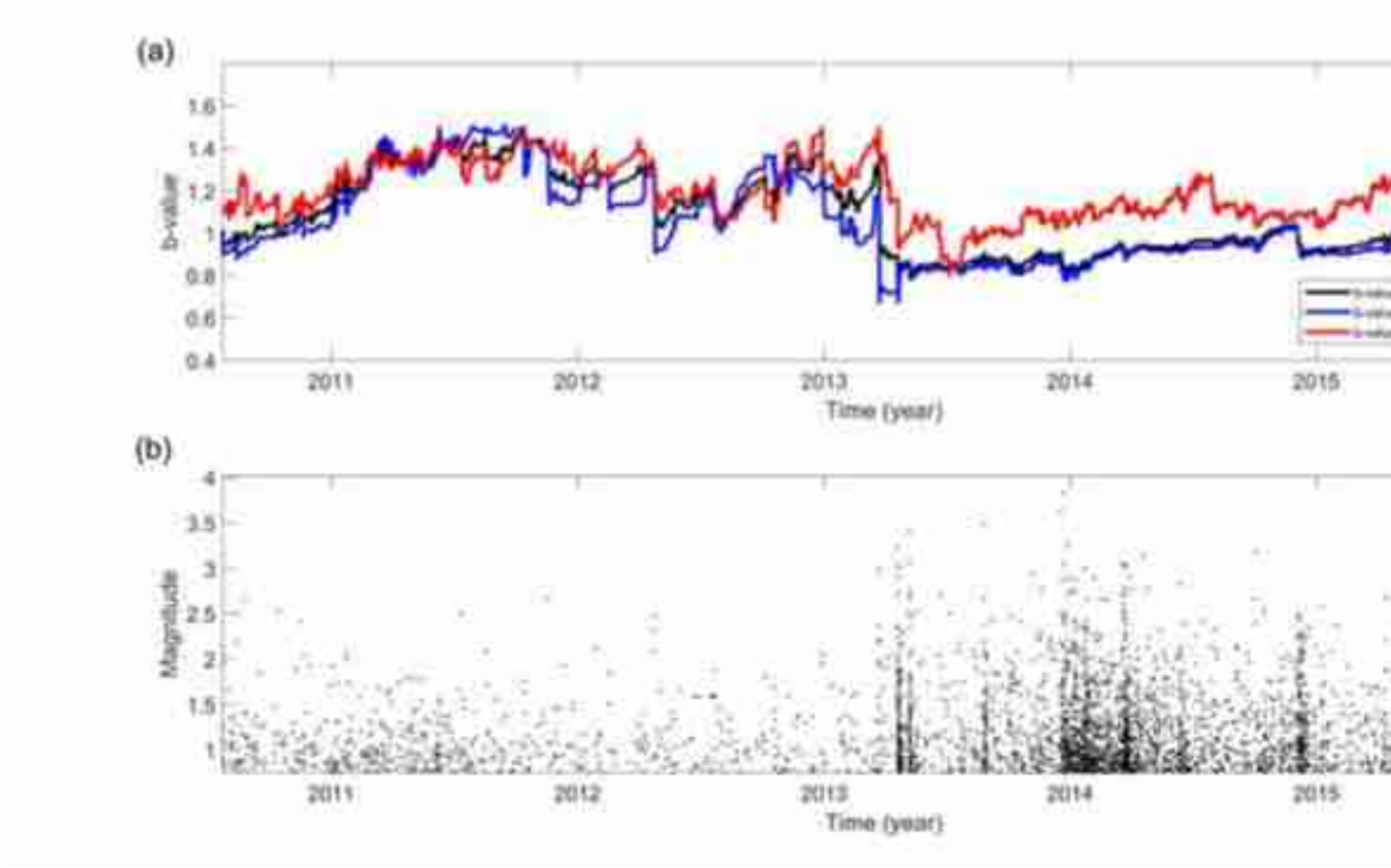

Figure S2

Click here to access/download;Supplemental Figures);FigureS2.jpg

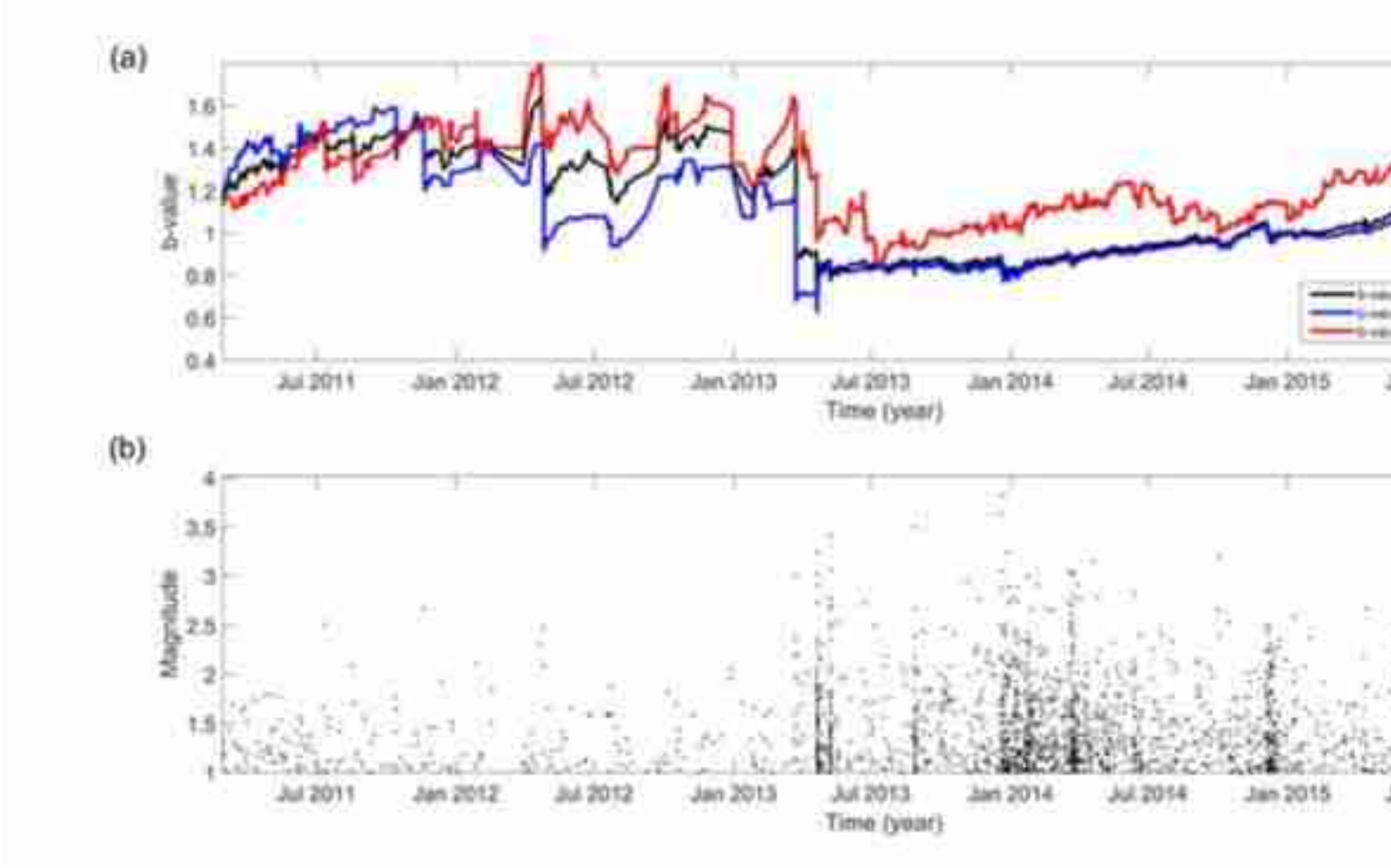

Figure S3

Click here to access/download;Supplemental Figures);FigureS3.jpg